UNIVERSITÀ DEL SALENTO

Marco Scigliuzzo

Optimization of SAW Filters and Resonators

Master's Thesis

Supervised by
Prof. Giuseppe Maruccio
Dott. Pasquale Scarlino
Dott. Silvia Rizzato

Università del Salento
February 2016

UNIVERSITÀ DEL SALENTO
Facoltà di scienze matematiche fisiche e naturali
Corso di laurea in Fisica Magistrale

Optimization of SAW Filters and Resonators

Master's thesis

Supervised by
Prof. Giuseppe Maruccio
Dott. Pasquale Scarlino
Dott. Silvia Rizzato

Candidate
Marco Scigliuzzo

Special Session - Academic Year 2014-2015

To my Grandmother, who would have liked to see this thesis more than anything, and to my Mother, who shares her desire.

CONTENTS

NOMENCLATURE

α, β	Lamè constants
$\approx$	approximately equal to
$\Delta\phi$	phase acquired by a wave in a cavity
δ_{ij}	kronecker delta
λ	Wavelength
$\mathbf{r}$	General radius vector
$\mathbf{u}$	Displacement vector
ϕ_g	phase acquired by a wave after a mirror reflection
ρ	mass density
σ_{ij}	Stress tensor components
$\sim$	Order of magnitude
C	Dynamic capacity due to SAW
C_0	Static capacity of an IDT
c_{ijkl}	Elasticity tensor components
c_{ij}	Elastic matrix components
f	Frequency
f_0	Center frequency
f_1	first lateral mode in a cavity
g	Gap between mirror ends and fornt of the SAW
h	Metal layer thickness
K	Electromechanical coupling
L	Dynamic inductance due to SAW
L_c	Total cavity dimension
l_m	mirror stripe length

L_p	Penetration length
l_p	IDT pairs length
n_g	number of gratings
n_p	number of pairs in IDT
n_w	number of stationary waves in a cavity
Q	Total quality factor
Q_0	Internal Quality Factor
Q_e	External Quality Factor
R	Dynamic resistance due to SAW
r	reflection coefficient for a single strip
r_e	electrical reflection coefficient for a single strip
r_m	mechanical reflection coefficient for a single strip
s_{ij}	Strain tensor components
t	transmission coefficient for a single strip
u_i	Displacement vector components
v	free wave velocity
v_m	Metalized wave velocity
Z	SAW resonator impedance
Z_0	Feed line impedance
IDT	Inter-digitate Transducer
PCB	Printed Circuit Board
RAM	Reflective Array Model
RF	Radio Frequency
SAW	Surface Acoustic Wave

ACKNOWLEDGEMENTS

Acknowledgements are difficult. Authors often enumerate and thank a list of people for their help, and with the same frequency these lines are skipped by each reader that does not have any relationship with the writer: simply because nothing is said about the entire work. I will try something different: this is the "people's" story of this thesis.

It was the end of July and I was studying for my last exam when suddenly a good friend of mine, Pasquale, came up with an idea: he wanted me to study SAW devices for my thesis. Few days later I met my supervisor, Giuseppe, and he suggested me a project for this topic. At the same time another professor, Dario, told me about his idea of simulation of Casimir effect in fluid. I felt torn between the two. That evening I had a phone conversation with my friend Gabriele; it lasted two hours, and we mainly talked about my doubts: he helped me a lot, but I was still unsettled. The next morning I spoke to my mother: in her opinion I had already made a decision. And the same day, my friend Alice gave me the same verdict: probably they knew something that I did not. Some days later, I had lunch at my friends', Valentina and Antonella, house, with Adalberto and Elisa; none of them are used to scientific subjects, so I exposed my difficulties from a different point of view, the emotional one.

The day of my last exam I made up my mind: I think you know what it is. That day a continuous uninterrupted flow of emails, articles, thesis, ideas and phone calls from Pasquale began.

The next morning it was my first day in the laboratory, there I met Silvia, Annagrazia and Angelo, part of Giuseppe's research group. I also met Fulvio, that was writing report for an annual exam. Annagrazia showed us how to use the instruments. There were simple ones, that could work just by pressing buttons, and difficult instruments, like the bonding machine, that could or could not work: Annagrazia spent an entire afternoon to show and teach us how to use them, and to let us make some try on test samples. At the end of my first day I was exhausted, I had been focused on the training for twelve hours: as soon as I arrived at home I went directly to bed. The next day I found out that my friend Francesca, who have tried unsuccessfully to call me the previous day, had speculated about my disappearance in thousands of ways. I worked with Silvia and Fulvio for a week,

then we stopped for the summer break. From that moment on Pasquale vanished: no more phone calls, no emails, no messages.

The holiday was great: the exam-free feeling made me approach everything with a different perspective. When my friend Francesco, who had been asking for a year about my exams, knew that I had begun my thesis he told me: "era ura" (a colorful expression that means finally). My friend Marco joked about the possibility of getting rich with my work (he is not accustomed to a physicist's salary). That summer did not last very long, but I spent a very good time with all my old friends Simone, Alessia, Matteo, Lara, Marco, Daniela, Emanuele, Giulia, Fiordi, Alessandro, Stefano, Gianni, Pietro, Marta, Edoardo, Lucrezia, Silvia, Adalberto, Elisa. They all are from different study fields, so I tried to explain them what I was doing, and why I was so exited about that. An evening I had dinner with my friends from the university, Gabriele, Alice, Francesca, Giorgio and Marta: it was a delightful meeting, we have not seen each other for a long period of time, and finally I had something interesting to say (instead of "I'm studying for an exam"). Another evening I met my old friend from ISUFI: Caterina, Marco, Michela, Alberto, Marco, and Pasquale who out of the blue turned up again. Marco and Alberto was interested in my thesis, and we discussed about the possibility of my project. But after some time we ended up arguing around some philosophical matters. Few days later I went to Otranto, an impressive city on the Adriatic coast, with my friend Caterina, Alice, Chiara, Francesca, Adalberto, Francesco, Elisa, Pietro, Marta and Edoardo: we did not talk about my thesis, but we walked, for a long trip (they remember why...and how it ended). I spent my last day of holiday with Chiara, and my new friends Chiara and Annalisa: We had a peculiar trip in Porto Selvaggio, a Ionic sea shore and that night We went at a music festival "La notte della Taranta". I have to thank Stefano for the wine that gave me a very good mood.

The next Monday I was in the laboratory, with the special presence of Pasquale. We talked to Giuseppe in order to figure out which way we would have proceeded. Giuseppe pointed out that his brother works with piezoelectric mechanic simulation, therefore few days later I met Claudio. The idea was to proceed in parallel with experimental and simulation study. The work progressed quickly, but, as always, there were some problems: for example, for the simulation I would have needed a supercomputing facility. Silvia and I drew the mask for the laser lithography: on a Sunday evening, when it was almost finished, I texted her that perhaps we made a mistake. The next day she told me that

she immediately stopped her work on the mask. Few days later we finished the mask, and Giuseppe gave us the "OK" to proceed with the fabrication.

This step was not as smooth as I had planned; it took two weeks to complete the process: for some reasons the lift-off wasn't really successful. In some fingers there were metallic shorts, that were really tough to remove with acetone. I called Silvia about 1000 times asking for news until the new samples were ready: I think she hated me in that period. In the meantime I studied the theory of piezoelectricity, I began to set the simulations, and I started to write this thesis.

When the new lift-off finished we had lost half of our devices, but at least we could begin to measure new samples. I soldered 2 new PCBs: my father brought me a desoldering pump to try to reuse the old PCB, but we decided to use only the new ones. In 3 days we measured a dozen of IDT filters with different features: fortunately the results were as expected and Silvia wrote a little presentation to show Giuseppe the results. That Friday morning I arrived in the laboratory, and I saw Annagrazia and Silvia focused on the preparation of some educative experiments; they also let me know that the university would organize a public event that night, "La Notte dei Ricercatori", where scientific researchers would meet the public and show their work. I spent the entire day with them, and it was a very pleasing and gratifying experience.

After few days we had a general meeting with all group members in order to understand how to move on. There were Silvia, Annagrazia, Serena, Giuseppe, Claudio, Vittorianna, and Pasquale via Skype. They were the beginning of October, and we decided to design and fabricate the resonators on GaAs and then move to new substrates; but there was a problem: the chiller of the Clean Room was broken, and we cannot launch any process. But every cloud has a silver lining, so we decided to set up a new measure configuration. The next day Giuseppe helped us to mount the apparatus, and we began to take new measurements. I was very excited because I could directly compare them with my simulation results.

During that week I spent at least 10 hours a day in the lab, and in the evening I was very tired. But when I finished my work before the 8 pm, I got used to go and visit my friends at their accommodations in the University campus. Mariapia was the most common victim, but Gabriella, Adele and Antonella faced the same destiny: I could not spend too much time, but those small talks restored me after the whole day in the lab. A Friday night i was talking to Stefano about the very demanding tasks

i had to accomplish in this type of activity: I remember I was exhausted but also glad and joyful. Stefano told me I was lucky, because 99% of people don't have the job of their dreams.

When the chiller was fixed, we run the mask that we designed.

I do not know if you have reached this point; if so, I have to apologize! Now I am running late and I prefer reviewing twice the thesis than finishing this story. I would have liked to tell you about how I met Francesco and Marco when I fixed the mask generator computer,or about my father who brought me his tools from home every time I needed, or about the excitement about the good results, or finally about the fight with Adalberto and my friends, because of the many hours I spent in the lab. In any case you are always free to ask, but as you read here, it is not a short story.

ABSTRACT

This work concerns the optimization of surface acoustic waves (SAW) devices on piezoelectric crystal materials and the investigation of SAW propagation and resonant modes in these systems.

Surface acoustic waves are mechanical waves that can be excited only at interfaces of a solid. They are a combination of share and longitudinal waves, since the material is stretched in both directions of wave propagation and perpendicular to the surface. They are called surface waves because the strain decreases exponentially with distance from surface, and usually the penetration length is about a wavelength.

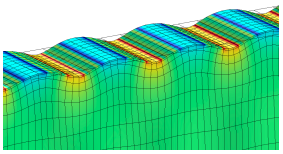

Surface Acoustic Wave (SAW) produced on a piezoelectric substrate by applying an oscillating potential to interdigital electrodes.

Piezoelectric materials are solid bodies where the deformation and the electric field are coupled: an electric field produces a strain and a strain produces an electric field. These materials are suitable for our task because an oscillating electric field can efficiently generate a mechanical perturbation: a particular shape of electrode, called **interdigitate transducer** (IDT) can produce a SAW. The IDT consists of a series of metallic lines: when an oscillating potential is applied, each couple of consecutive lines behave as a capacitor, producing an electric field that deforms the piezoelectric substrate.

Interdigitate transducer (IDT) electrodes on piezoelectric substrate.

The piezoelectricity can be shot down for a short distance from the surface, depositing a metallic layer. A deformation of this structure needs the same amount of energy for the elastic deformation, but does not require anymore the electrostatic energy to produce the electric field: a piezoelectric material with a thin layer of metal on its surface is less stiff than before. As a result there is a different propagation velocity of waves for piezoelectric material covered by a metal, which correspond to a change in the index of refraction experienced by the propagating wave for the transition during its transition between the metallized part to the free one. Therefore periodic structure of different index of refraction can be used in order to obtain Bragg reflectors. Two of these mirrors in series make a cavity, where the confined SAW can interfere constructively.

A SAW brings an electric field as it propagates; the velocity of a SAW is about 3000 $\frac{m}{s}$, 5 order of magnitude smaller than the light speed: the coupled electric field is driven completely by the

mechanics propagation, and obey to electrostatic equations. This field can be coupled with other physical system.

In this thesis the SAW devices are investigated, in the form of filters and resonators on **bulk GaAs** and an heterostructure of **GaN on sapphire**. The devices are fabricated with photolithography with features usually at optical limit i.e. $\sim 1\mu m$.

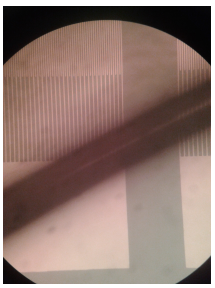

Hair on IDT.

A preliminary study on GaAs was carried out in order to understand the best geometry suitable for the filters: a range of different **number of electrodes pairs** in the IDT, **distances** between emitter and receiver and IDT **shapes** are examinated. The results gave the direction for the design of the resonators emitters.

Another study of resonators on GaAs was carried out using a range of different number of electrodes in the Bragg reflectors and in the emitter, different electrodes lengths and different distances between the Bragg reflector.

The best devices were selected for a systematic study of the **Q-factor** of resonators on GaAs. At the same time these devices were tested with a light source that promotes electrons in the conduction band. Moreover the best filters and resonators were fabricated on the GaN heterostructure.

Finally a simulation of filters and resonators with **finite elements method** (FEM) was conducted.

1

THEORY OF SURFACE ACOUSTIC WAVES

Surface acoustic waves (SAW) are mechanical oscillations traveling on the surface of an elastic material, whose amplitude decrease exponentially with depth. Since they are a combination of longitudinal and shear waves, there are two kinds of SAW: **Rayleigh waves**, when the shear plane is normal to the surface, and **Love waves**, when the shear plane is parallel to the surface. From now on we refer only to Rayleigh waves.

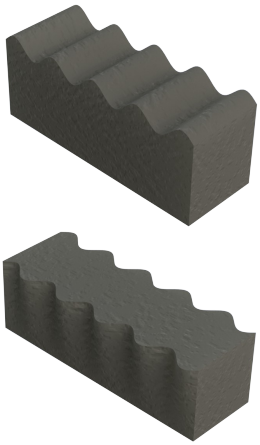

Rayleigh and Love waves (top and bottom of the figure respectively).

SAW solutions of motion equations can be obtained easily in isotropic elastic materials; these solutions also exist for anisotropic elastic materials and for piezoelectric ones, but in these cases there are difficulties due to the higher dimensions of the problem (for example the wave dispersion relation becomes a secular equation). Moreover the search for boundary conditions that excite a SAW on a piezoelectric material can be often studied only with perturbative techniques [7], or with numerical methods.

For these reasons in this chapter we briefly give a simple unidimensional treatment for SAW devices, that is enough for understanding the chapter 2 on experimental setup and the chapter 3 on measurements. Then a more detailed study on the physics of SAW is carried on. This part is fundamental for reading chapter 4 on numerical solutions of motion equations, because it explains the dynamics SAW on piezoelectric materials.

1.1 OVERVIEW ON SURFACE ACOUSTIC WAVE

In this section a simplified unidimensional treatment of surface acoustic waves is presented in order to give an idea of the phenomenon. Firstly the motion equations are derived, in order to make the reader comfortable with the dynamics of the SAW, then it is shown how a particular shape of electrode can excite these waves and interact with them.

1.1.1 *Unidimensional mechanical equations*

Applying a force F to a solid body of length l and lateral area A, a displacement Δl occurs. For small deformation, $\frac{\Delta l}{l} \ll 1$, the

displacement is proportional to the force and the **Hooke's law** holds:

$$F = k\Delta l, \tag{1.1}$$

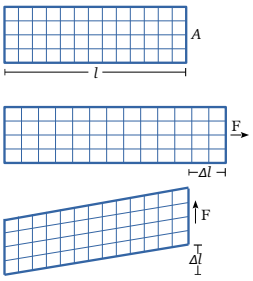

Linear deformation of an elastic body.

where k is the **elastic coefficient**. For an anisotropic material, different directions of the force correspond to different values of k, but let us consider a fixed direction. k depends on the total length l and on the area A: in fact two equal bodies in series lead to doubling the displacement for the same amount of force, and for two equal bodies in parallel we expect the half. Therefore it is useful to consider the elastic constant for unit length and unit area. Defining the **stress** σ as the force per unit area

$$\sigma = \frac{F}{A}, \tag{1.2}$$

and the strain s as the displacement per unit length:

$$s = \frac{\Delta l}{l}, \tag{1.3}$$

The order of magnitude for elastic constant is 10^{11} Pa. In order to strain of 1% a cube of 1m of side, a force of 10^9N is needed.

the Hooke's law can be written as:

$$\sigma = \frac{kl}{A}s = cs, \tag{1.4}$$

where c is called **elastic constant** and it is measured in Pascal.

If the force F applied to the body depends on time, so does the displacement $\Delta l = u(x,t)$. Therefore it is possible to excite mechanical waves in an elastic solid. Applying third Newton law to displacement we obtain:

$$F = m\partial_t^2 u \qquad \Rightarrow \qquad \frac{F}{V} = \frac{\sigma}{l} = \rho\partial_t^2 u. \tag{1.5}$$

Using the Hooke's law and taking the limit for infinitesimal body ($l \to 0$):

$$\begin{cases} \dfrac{\sigma}{l} \to \partial_x \sigma \\ s = \dfrac{u}{l} \to \partial_x u \end{cases} \qquad \Rightarrow \qquad \partial_x \sigma = c\partial_x s = c\partial_x^2 u = \rho\partial_t^2 u \tag{1.6}$$

and we then obtain the **wave equation**:

$$\partial_x^2 u - \frac{c}{\rho}\partial_t^2 u = 0. \tag{1.7}$$

The density ρ of a solid body is about $10^4 \frac{kg}{m^3}$ so that the magnitude order of speed of sound is around $3 \cdot 10^3 \frac{m}{s}$.

This is a linear non dispersive and non dissipative equation. The sound of speed is

$$v = \sqrt{\frac{c}{\rho}}. \tag{1.8}$$

1.1.2 *Unidimensional Piezoelectric Equations*

When a body is placed in an electrical field **E** a displacement of its charged microscopic components from their equilibrium position takes place. As a consequence an additional electrical field appears due to the local polarization **P** of the material. This field is equal to the one produced by a local charge density

$$\rho = -\nabla \cdot \mathbf{P}. \tag{1.9}$$

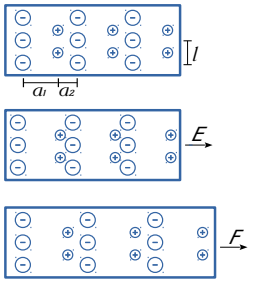

Effect of electric field and displacement on a ferroelectric material.

So we take into account this contribution defining the **displacement field**:

$$D = \epsilon E. \tag{1.10}$$

For semplicity let's consider a ferroelectric crystal, like in the picture. Suppose that the elementary charge is q, that the elementary cell width is l and that the elementary cell length is $a_1 + a_2$, where a_1 is the distance between anion and cation (see the figure on this page). The density of dipole moment is

$$P = \frac{p}{V} = \frac{q(a_2 - a_1)}{l^2(a_2 + a_1)}. \tag{1.11}$$

If the material is strained the displacement of atoms $\Delta a_1 = a_1 s$ and $\Delta a_2 = a_2 s$ produces a change of

$$\Delta P = Ps = es, \tag{1.12}$$

Considering $a_1 1\cdot \sim 10^{-10}\,m$, $a_2 \sim 2 \cdot 10^{-10}\,m$ *and* $l \sim 3 \cdot 10^{-10}\,m$, $q \sim 10^{-19}\,C$ *then* $e \sim 1\,\frac{C}{m^2}$.

where e is called **piezoelectric constant**. Therefore the displacement field becomes:

$$D = \epsilon E + \Delta P = \epsilon E + es. \tag{1.13}$$

The stresses on the region of length a_1 and a_2 are respectively:

$$\sigma_1 = \frac{qE}{l^2} \quad \text{and} \quad \sigma_2 = \frac{-qE}{l^2}, \tag{1.14}$$

therefore the average stress due to electric field can be calculated using the proportion of the fraction of total elementary cell on which these stresses are applied:

$$\sigma_E = \sigma_1 \frac{a_1}{a_1 + a_2} + \sigma_1 \frac{a_2}{a_1 + a_2} = \frac{a_1\sigma_1 + a_2\sigma_2}{a_1 + a_2} = eE; \tag{1.15}$$

finally using the elastic equation to total stress, i.e. the sum of externally applied stress and the electric stress $\sigma + \sigma_E = cs$:

$$\sigma + \sigma_E = cs \quad \Rightarrow \quad \sigma = cs - eE. \tag{1.16}$$

So we have the linear equations for piezoelectricity:

$$\begin{cases} D = \epsilon E + es. \\ \sigma = cs - eE \end{cases}. \tag{1.17}$$

Consider now the wave propagation in an infinite piezoelectric media: because there is no free charge the divergence (that is z derivative because it is a unidimensional system)

$$\partial_z D = 0, \tag{1.18}$$

so that D is constant in space or zero. This implies that the displacement current

$$i = \partial_t D \tag{1.19}$$

must be uniform or null. As we are considering just the piezoelectric media, without electrode, the current must be zero, and then $D = 0$. The piezoelectric equations then become:

$$\begin{cases} E = -\dfrac{es}{\epsilon} \\ \sigma = c\left(1 + \dfrac{e^2}{c\epsilon}\right) s \end{cases}, \tag{1.20}$$

therefore we can define an equivalent elastic coefficient:

$$c_e = c\left(1 + \frac{e^2}{c\epsilon}\right) > c. \tag{1.21}$$

A piezoelectric material is stiffer than an equivalent material that presents the same elastic coefficients but does not have the piezoelectric ones. Moreover remembering the wave velocity equation (1.8), a wave travels faster in a piezoelectric material. This conclusion can be explained considering that if a material is piezoelectric, when it is stretched it creates an electric filed; therefore the energy needed to deform such a material is the sum of the elastic energy stored in the deformed atoms bond, and the electric energy stored in the filed. If a non-piezoelectric material with the same elastic constant of a piezoelectric one exists, the amount of energy to stretch it is smaller, because it requires only the elastic energy.

1.1.3 *Interdigital Transducer and Bragg Mirror*

A Rayleigh wave can be exited on a piezoelectric substrate by using a particular shape of electrode: the **interdigital transducer** (IDT). This type of electrode is composed by a series of thin

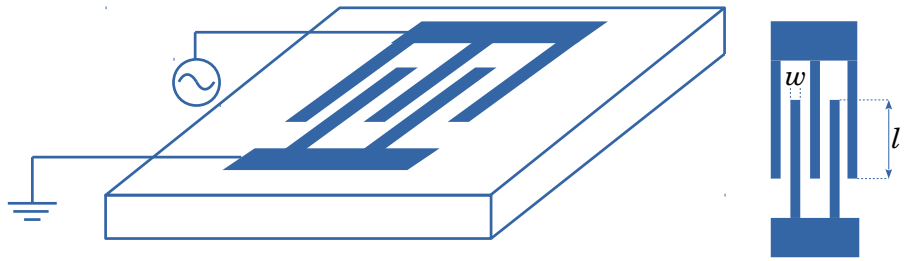

Figure 1.: *General shapes of IDT.*

metallic stripes, usually called **fingers**, connected alternatively to ground and to an oscillating signal, as shown in figure 1.

The stripes have a width w and are separated by the same distance, forming n_p pairs. The active part of this electrode is the region where the fingers superpose, whose length is l_p: in this region the stripes form a "series of capacitor" that creates an electric field that deforms the piezoelectric substrate. This deformation has a periodicity equal to $\lambda = 4w$. If an oscillating signal is applied, such that its frequency f matches the periodicity in order to satisfy the wave relation $\lambda f = v$, then a surface wave is generated.

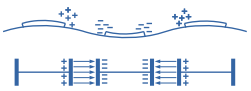

Working principle of IDT.

In order to understand the amplitude of these waves, we can follow this simple capacitor model. Each finger is distant w and the maximum applied voltage is V. The electric field between the fingers is $E \sim \frac{V}{w}$. As the surface is free there is no stress, and therefore the strain is:

$$cs - eE = 0 \Rightarrow s = \frac{e}{c}E. \tag{1.22}$$

Since the penetration length is $\sim \lambda$, the strain is applied for the same amount of distance, therefore the **wave amplitude** is

Considering distance between fingers $\sim 1\mu m$ *and voltage* $\sim 1V$*, the electric field is* $E \sim 10^6 \frac{V}{m}$*. This give strain of* $\sim 10^{-6}$ *and amplitude of* $\sim 0.1nm$.

$$A \sim 4w\frac{e}{c}\frac{V}{w} = 4\frac{e}{c}V. \tag{1.23}$$

This is the amplitude caused by a single pairs; in the IDT there is a **constructive effect**: a peak created by a pair travels to the next pair that enhances its amplitude, and then to another pair again, and again for n_p times. Of course the effect is not linear (double n_p does not double the final amplitude). In our devices this effect saturates at $n_p \approx 100$ (see section 3.1.2 and figure 17 in particular).

A Rayleigh wave can be reflected by a metallic stripe placed on the surface of the piezoelectric material. When a piezoelectric material is coated with metal,but the electric field $E = 0$ in all di-

rection but the z one. The piezoelectric relation for stress becomes

$$\sigma = cs - eE \quad \Rightarrow \quad \sigma = cs, \tag{1.24}$$

that is the same for elastic materials. Therefore a **metalized piezoelectric** is less stiff than the free one. As a consequence the wave propagates with a smaller velocity v_m under a metallic layer. Since a traveling wave meets a discontinuity, a fraction of it is reflected. It is possible to give an idea of the order of magnitude of reflection considering the **electromechanical coupling** K:

$$\frac{K^2}{2} = \frac{\Delta v}{v} = \frac{v - v_m}{v} = 1 - \frac{v_m}{v} \tag{1.25}$$

Using the equation (1.8) with the elastic constant c for the metalized piezoelectric, and the equivalent elastic constant c_e for the free one, the ratio

$$\frac{v_m}{v} = \sqrt{\frac{1}{1 + \frac{e^2}{c\epsilon}}}. \tag{1.26}$$

Because $\frac{e^2}{c\epsilon} \ll 1$ it is possible to approximate

$$\left(\frac{1}{1 + \frac{e^2}{c\epsilon}}\right)^{\frac{1}{2}} \approx \left(1 - \frac{e^2}{c\epsilon}\right)^{\frac{1}{2}} \approx 1 - \frac{1}{2}\frac{e^2}{c\epsilon}, \tag{1.27}$$

Remembering that ϵ in the SI unit is $\epsilon_0\epsilon$, for GaAs we have $K^2 \approx 6 \cdot 10^{-4}$.

so that the electromechanical coupling

$$K^2 = \frac{e^2}{c\epsilon}. \tag{1.28}$$

Except for few material, K^2 is always small , therefore a single metallic stripe reflects a tiny amount of the incident wave. In order to have a reflective electrode, it is possible to make a **Bragg mirror** stacking a considerable number of stripes in series, so that the waves reflected interfere constructively, and the reflection raises up to near the total incident wave. Considering a mirror

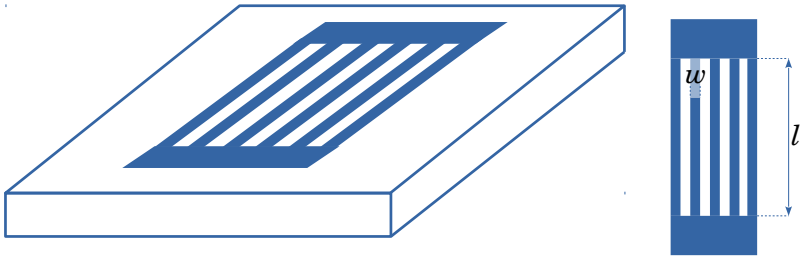

Figure 2.: *General shapes of Bragg mirror.*

like in figure 2, all length l_m of stripe reflects the wave, so that it is usually larger than the incident wave, in order to reduce diffraction effect. The number of gratings n_g is usually from 100 to 1000., i.e. 1 order of magnitude more than the IDT pairs. Keeping in mind that each stripe is micrometric, it is evident that a mirror is a "macroscopic" device with microscopic features.

1.1.4 *Filters and Resonators*

The wave excited by an IDT can be detected by another IDT: the deformations carry an electric field, whose signal is read by each stripes (see figure 3). The mechanical signal travels at sound speed, that is 5 order of magnitude smaller then the light one. For this reason 2 IDT placed one after the other are called **delay line**: an electromagnetic signal sent through a transmission line, slows down when it is converted in mechanical waves, and when it is changed back, it has a temporal delay proportional at the distance between the IDT.

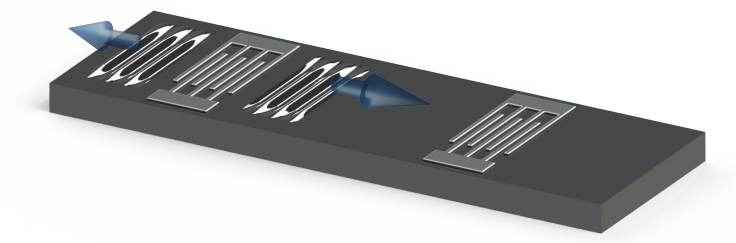

Figure 3.: *Impulse wave emitted by an IDT in opposite directions.*

For our devices $w \approx 2\mu m$ *and* $v \approx 3000\,\frac{m}{s}$, *therefore* $f_0 \approx 400MHz$.

The wavelength λ is fixed by finger width w, and because the wave velocity v is fixed by the substrate, the delay line works only at the frequency $f_0 = \frac{v}{\lambda}$. For this reason the delay lines are also called **filters**: when an electromagnetic signal is sent, only a specific frequency pass through.

f_0 is the most efficient frequency at which the IDT works. But there is a range of frequency where a signal is still transmitted: all these frequencies form the **bandwidth** of the filter.

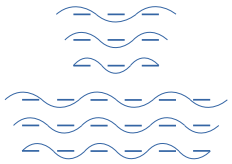

Bandwidth of an IDT.

Taking in mind the aim of this section, we only provide a simplified explanation of the correlation between number of pairs n_p and the bandwidth. When a RF signal is applied to the electrodes it charges the fingers. The oscillations are located on the fingers, while the SAWs nodes must be within the electrodes. At the resonance frequency, the nodes are exactly placed in the center among the fingers. The bandwidth can be calculated by considering an additional shift of $\Delta\lambda$ at each node. In order to respect

the condition of nodes between the finger, the maximum value of this shift is

$$\Delta\lambda = \frac{\lambda}{n_p}, \tag{1.29}$$

Differentiating the wave relation $f = \frac{v}{\lambda}$:

$$|\Delta f| = \frac{v}{\lambda^2}\Delta\lambda = f_0\frac{\Delta\lambda}{\lambda}. \tag{1.30}$$

Our devices have $f_0 \sim 400MHz$ and $n_p \sim 40$, therefore the bandwidth $\Delta f \sim 10MHz$.

therefore the bandwidth is approximately

$$\Delta f = \frac{f_0}{n_p}. \tag{1.31}$$

The IDT produces two waves, traveling in opposite directions, so that half of the signal is lost. Moreover the receiver has a limited efficiency, and another fraction of the energy passes through it. As a consequence the read signal is always smaller then the emitted one.

The waves excited by an IDT can be reflected by a Bragg mirror. If two mirrors are placed in series and an IDT in between of them, the waves bounce from a mirror to the other. If the distance between mirrors is chosen to give constructive interference at each reflection, the signal enhances every reflection giving a resonance. This kind of device are therefore called **resonator**. Resonators are characterized by the **Q factor**:

$$Q = \frac{\text{energy lost per cycle}}{\text{total energy stored}}. \tag{1.32}$$

Roughly speaking this value gives how many oscillation a system can do before loosing all its energy; if a cycle lasts Δt and the system needs ΔT to relax, then:

$$Q = \frac{\Delta t}{\Delta T}. \tag{1.33}$$

The best resonators in this thesis have $Q \sim 10^4$.

The same reasoning can be used in the frequency space: if a cycle lasts Δt then its frequency if $f_0 = \frac{1}{\Delta t}$, and if a system needs ΔT to relax it has a bandwidth in frequency of $\Delta f = \frac{1}{\Delta T}$, then

$$Q = \frac{f_0}{\Delta f}. \tag{1.34}$$

As for the IDT, also a mirror has a bandwidth: the phenomenon is the same discussed for IDT, but in contrast the number n_g is so high that a mirror bandwidth is very narrow.

1.2 ELASTICITY

Following [2] and [1] we introduce the basic elements in the theory of elasticity: the **strain tensor** and the **stress tensor**, their relation through the **elastic tensor**, and their most significant relations with waves propagation in crystals.

1.2.1 *Strain Tensor*

The theory of elasticity treats solids bodies as continuous media. At equilibrium, each point of a body is identified by a vector $\mathbf{r}$ (with components x_i) and when a force is applied its position changes in $\mathbf{r}'$ (with components x_i'). We define $\mathbf{u}$, the **displacement vector**, as

Vectors and Tensors are not just simple numbers grouped together in order to simplify the notation. All vectors or all tensors of the same class respect the same specific rules of transformation.

$$u_i = x_i' - x_i. \tag{1.35}$$

Consider the distance between two points very close together: after the deformation the initial distance $dl = \sqrt{dx_i^2}$ becomes $dl' = \sqrt{dx_i'^2}$. Using the relation

$$dx_i' = dx_i + du_i = dx_i + \partial_j u_i dx_j, \tag{1.36}$$

the distance after the deformation can be written as

$$\begin{aligned} dl'^2 &= (dx_i + \partial_j u_i dx_j)^2 \\ &= dl^2 + 2\partial_j u_i dx_i dx_j + \partial_j u_i \partial_k u_i dx_j dx_k. \end{aligned} \tag{1.37}$$

If the deformation is small if compared to the body dimensions, this means that

$$\partial_i u_j \ll 1, \tag{1.38}$$

so that the last term in the previous formula can be neglected. Moreover the indexes i and j in the middle element of the previous expression are symmetric, so we can write

The strain tensor is symmetric, $s_{ij} = s_{ji}$ therefore only 6 of its elements are independent (3 diagonal and 3 out of diagonal).

$$\partial_j u_i dx_i dx_j = \partial_i u_j dx_i dx_j. \tag{1.39}$$

Defining the **strain tensor**:

$$s_{ij} = \frac{1}{2}\left(\partial_i u_j + \partial_j u_i\right), \tag{1.40}$$

the distance after deformation becomes

$$dl'^2 = dl^2 + 2s_{ij} dx_i dx_j. \tag{1.41}$$

The strain tensor is a dimensionless quantity that describe the relative deformation in each point of a solid body.

1.2.2 *Stress Tensor*

The strain tensor describe the cinematic of deformation; in order to treat the dynamics we need to describe the forces in an elastic body. When deformations occur, internal forces, called **stresses**, arise to restore the original equilibrium position of the body. By integrating the force for unit volume **f** in the whole volume of a portion of a strained body, we get the amount of force **F** on that portion:

$$\mathbf{F} = \int \mathbf{f} dV. \tag{1.42}$$

Piezoelectricity is due to Electric field, that is long range interaction. We see later how to deal with this kind of forces.

The internal stresses are due to molecular interactions, and therefore they are treated as **short range** interactions. This means that each force on a portion of a body is applied through its surface. Therefore the previous expression can be calculated integrating the contribution of force applied on a surface, for each direction:

$$F_i = \int \sigma_{ij} dS_j, \tag{1.43}$$

where σ_{ij} is called **stress tensor**, and describe the force for unit surface, directed in i direction, and applied on a surface with normal j. It can be shown that this is a symmetric tensor:

The condition that only superficial forces can produce a moment on a portion of the body implies the stress tensor is symmetric.

$$\sigma_{ij} = \sigma_{ji} \tag{1.44}$$

Mathematically we can introduce the stress tensor applying the **divergence theorem** to expression (1.42):

$$\int f_i dV = \int \partial_j \sigma_{ij} dV = \int \sigma_{ij} dS_j, \tag{1.45}$$

where we notice that the volume forces can be expressed by stress tensor:

$$f_i = \partial_j \sigma_{ij}. \tag{1.46}$$

1.2.3 *Elastic Tensor and Hooke Law*

Let's focus our attention now on the work δW produced by the stress when a small deformation δu_i occurs:

$$\delta W = \int f_i \delta u_i dV = \int \partial_j \sigma_{ij} \delta u_i dV. \tag{1.47}$$

Integrating by part, δW can be written as

$$\delta W = \int \sigma_{ij} \delta u_i dS_j - \int \sigma_{ij} \partial_j \delta u_i dV. \tag{1.48}$$

The first integral in the previous expression vanishes when it is evaluated at the surface of an infinite body (where $\sigma_{ij} = 0$). The second integral can be reshuffled by virtue of symmetry of stress tensor:

$$\begin{aligned}\delta W &= -\frac{1}{2}\int \sigma_{ij}\left(\partial_i \delta u_j + \partial_i \delta u_j\right) dV \\ &= -\frac{1}{2}\int \sigma_{ij}\delta\left(\partial_i u_j + \partial_i u_j\right) dV = -\int \sigma_{ij}\delta s_{ij} dV.\end{aligned} \tag{1.49}$$

The elastic potential energy per unit of volume U is a state function:

$$W = \int_A^B dU = U_B - U_A; \tag{1.50}$$

this means that a variation of potential energy depends only on the deformation tensor at the initial and final state. So that

$$dU = \frac{\partial U}{\partial s_{ij}} ds_{ij}. \tag{1.51}$$

Comparing this with the equation (1.49) we see that

$$\frac{\partial U}{\partial s_{ij}} = \sigma_{ij}. \tag{1.52}$$

Expanding the potential energy in Taylor series near the equilibrium until the first non-zero term we have

In the expansion 0 stands for $s_{ij} = 0$.

$$\begin{aligned}U =& U(0) + \left.\frac{\partial U}{\partial s_{ij}}\right|_0 s_{ij} + \frac{1}{2}\left.\frac{\partial^2 U}{\partial s_{ij}\partial s_{kl}}\right|_0 s_{ij}s_{kl} \\ &= \frac{1}{2}c_{ijkl}s_{ij}s_{kl},\end{aligned} \tag{1.53}$$

where c_{ijkl} is called **elastic tensor**. Applying equation (1.52) to (1.53) we obtain the **Hooke's law**

$$\sigma_{ij} = c_{ijkl}s_{kl}, \tag{1.54}$$

that states the linear behavior between deformations and stresses in a solid body. The elastic tensor has $3^4 = 81$ components, but by virtue of the symmetry of s_{ij} we can write

$$c_{ijkl} = c_{jikl} = c_{ijlk} = c_{klij}; \tag{1.55}$$

as consequence there are only 21 independent components. It is convenient to exploit the symmetry introducing the **Voigt notation** for stress tensors:

$$\underbrace{\begin{pmatrix}\sigma_{xx} & \sigma_{xy} & \sigma_{xz}\\ \sigma_{yx} & \sigma_{yy} & \sigma_{yz}\\ \sigma_{zx} & \sigma_{zy} & \sigma_{zz}\end{pmatrix}}_{\text{tensor notation}} \longrightarrow \underbrace{(\sigma_{xx}, \sigma_{yy}, \sigma_{zz}, \sigma_{yz}, \sigma_{xz}, \sigma_{xy})}_{\text{Voigt notation}}, \tag{1.56}$$

and for strain tensor:

$$\underbrace{\begin{pmatrix} s_{xx} & s_{xy} & s_{xz} \\ s_{yx} & s_{yy} & s_{yz} \\ s_{zx} & s_{zy} & s_{zz} \end{pmatrix}}_{\text{tensor notation}} \longrightarrow \underbrace{(s_{xx}, s_{yy}, s_{zz}, 2s_{yz}, 2s_{xz}, 2s_{xy})}_{\text{Voigt notation}}, \tag{1.57}$$

The different representation for σ and s preserves the scalar invariance $\sigma_{ij}s_{ij} = \sigma_i s_i$.

With this notation the Hooke's law (1.54) becomes

$$\sigma_i = c_{ij}s_j, \tag{1.58}$$

where c_{ij} is a 6x6 symmetric matrix called **elastic matrix**.

1.3 SAW ON ELASTIC MATERIALS

Using the equation (1.46) and the second law of dynamics:

$$\rho\ddot{u}_i(\mathbf{x}, t) = \partial_j\sigma_{ij}. \tag{1.59}$$

Using the symmetry $c_{ijkl} = cijlk$, the Hooke's law (1.54) becomes

$$\sigma_{ij} = c_{ijkl}\partial_l u_k, \tag{1.60}$$

and the equations of motion

$$\rho\ddot{u}_i(\mathbf{x}, t) - c_{ijkl}\partial_j\partial_l u_k = 0. \tag{1.61}$$

These equations will be solved for an isotropic material, in order to fix ideas and to underline the physical dynamics.

Following [5], for an **isotropic** material the elastic constants become:

$$c_{ijkl} = \alpha\delta_{ij}\delta_{kl} + \beta(\delta_{ik}\delta_{jl} + \delta_{il}\delta_{jk}), \tag{1.62}$$

where α and β are the **Lamè constants**. Using this expression in the motion equations

$$\rho\partial_t^2 u_i = (\alpha + \beta)\partial_i\partial_j u_j + \beta\partial_j\partial_j u_i. \tag{1.63}$$

The presence of boundary condition, i.e. of a surface, is necessary for the SAW solutions of motion equations.

The ansatz of plane waves in the bulk requires no boundary condition, using

$$u_i = u_{0i}\exp\left(i(\omega t - \mathbf{k}\cdot\mathbf{x})\right), \tag{1.64}$$

we find the dispersion relation

$$\rho\omega^2 u_i = (\alpha + \beta)^2 k_i k_j u_j + \beta|\mathbf{k}|^2 u_i, \tag{1.65}$$

that divided for $\exp\left(i(\omega t - \mathbf{k}\cdot\mathbf{x})\right)$, and written with vector notation $\mathbf{u_0}$ is

$$\rho\omega^2\mathbf{u_0} = (\alpha + \beta)(\mathbf{k}\cdot\mathbf{u_0})\mathbf{k} + \beta|\mathbf{k}|^2\mathbf{u_0}. \tag{1.66}$$

Taking $\mathbf{u}_0$ perpendicular to $\mathbf{k}$ we have the **share waves**:

$$|\mathbf{k}_t|^2 = \omega^2 \frac{\rho}{\beta}, \tag{1.67}$$

where $\mathbf{k}_t$ is the wave number for share waves, and their velocity is

$$v_t = \sqrt{\frac{\beta}{\rho}}. \tag{1.68}$$

$\mathbf{u}_0$ can be in any direction perpendicular to $\mathbf{k}_t$.

Taking $\mathbf{u}_0$ parallel to $\mathbf{k}$ we have the **longitudinal waves**:

$$|\mathbf{k}_l|^2 = \omega^2 \frac{\rho}{\alpha + 2\beta}, \tag{1.69}$$

where $\mathbf{k}_l$ is the wave number for longitudinal waves, and their velocity is

$$v_t = \sqrt{\frac{\alpha + 2\beta}{\rho}}. \tag{1.70}$$

Since α and β are always positive:

$$v_l > v_t, \tag{1.71}$$

the longitudinal waves travel always faster than the shear ones.

Consider now an infinite solid body with a surface parallel to the plane x_1x_2 and located at $x_3 = 0$. A SAW that travels in the x_1 direction with periodicity k_r has the formal velocity (because at this point it is only a formal expression):

$$v_R = \frac{\omega}{k_R}. \tag{1.72}$$

The equations of motion are the same, but now we must add the boundary condition

$$\sigma_{i3}(x_3 = 0) = 0, \tag{1.73}$$

that means that the surface is free. The ansatz combines both shear and longitudinal waves:

$$\mathbf{u}_R = A\mathbf{u}_l + B\mathbf{u}_t, \tag{1.74}$$

where A and B are the constants of the linear combination: these waves are called the **Rayleigh waves**.

Since they travel in the x_1 direction, there are no components along x_2 in the wave vectors:

$$\mathbf{k}_l = (k_R, 0, L) \quad \text{and} \quad \mathbf{k}_t = (k_R, 0, T), \tag{1.75}$$

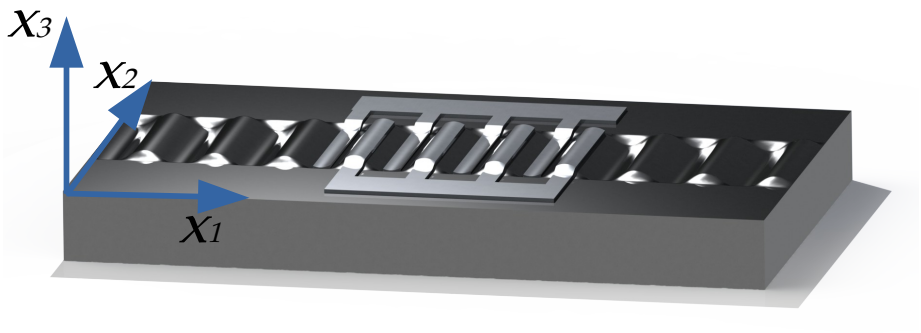

Figure 4.: *Rayleigh waves propagation direction.*

where L and T are constants that will be determined. Using the expressions derived before

$$|\mathbf{k}_l|^2 = \frac{\omega^2}{v_l^2} \quad \text{and} \quad |\mathbf{k}_t|^2 = \frac{\omega^2}{v_t^2}, \tag{1.76}$$

we can calculate the value of

$$L^2 = \frac{\omega^2}{v_l^2} - k_R^2 = \frac{\omega^2}{v_l^2} - \frac{\omega^2}{v_R^2} \quad \text{and} \quad T^2 = \frac{\omega^2}{v_t^2} - k_R^2 = \frac{\omega^2}{v_t^2} - \frac{\omega^2}{v_R^2}. \tag{1.77}$$

As the wave amplitude must decrease with the negative direction of x_3, both L and T are pure imaginary. From the previous expressions we can write

$$v_R < v_t \quad \text{and} \quad v_R < v_l, \tag{1.78}$$

i.e. Rayleigh waves are **slower** than both shear and longitudinal waves. The displacement vectors are therefore

$$\begin{aligned} \mathbf{u}_l &= (k_R, 0, L) \exp\left(i(\omega t - k_R x_1 - L x_3)\right) \\ \mathbf{u}_t &= (T, 0, -k_R) \exp\left(i(\omega t - k_R x_1 - T x_3)\right) \end{aligned}. \tag{1.79}$$

The total displacement $\mathbf{u}_R$ must respect the boundary condition; so that using Hooke's law we obtain

$$\begin{cases} \partial_1 u_{R3}|_{x_3=0} + \partial_3 u_{R1}|_{x_3=0} = 0 \\ \partial_2 u_{R3}|_{x_3=0} + \partial_3 u_{R2}|_{x_3=0} = 0 \\ \alpha \partial_i u_{Ri}|_{x_3=0} + 2\beta\ \partial_3 u_{R3}|_{x_3=0} = 0 \end{cases}, \tag{1.80}$$

that applied to

$$\begin{cases} u_{R1} = A k_R \exp\left(i(\omega t - k_R x_1 - L x_3)\right) + BT \exp\left(i(\omega t - k_R x_1 - T x_3)\right) \\ u_{R2} = 0 \\ u_{R3} = AL \exp\left(i(\omega t - k_R x_1 - L x_3)\right) - B k_R \exp\left(i(\omega t - k_R x_1 - T x_3)\right) \end{cases}, \tag{1.81}$$

gives the linear homogeneous system for A and B:

$$\begin{cases} B\left(k_R^2 - T^2\right) - 2Ak_RL = 0 \\ 2\beta Bk_RT - A\left((2\beta+\alpha)L^2 + \alpha k_R^2\right) = 0 \end{cases}. \tag{1.82}$$

The only non trivial solution is the one that makes the determinant equal to zero:

$$(k_R^2 - T^2)\beta\left(\frac{2\beta+\alpha}{\beta}L^2 + \frac{\alpha k_R^2}{\beta}\right) + 4\beta k_R^2 LT = 0, \tag{1.83}$$

and using the definition of L^2 we can write:

$$(k_R^2 - T^2)^2 - 4k_R^2 LT = 0. \tag{1.84}$$

By substituting the expressions for L and T we have

$$\left(2 - \frac{v_R^2}{v_t^2}\right)^2 = 4\sqrt{1 - \frac{v_R^2}{v_t^2}}\sqrt{1 - \frac{v_R^2}{v_l^2}}. \tag{1.85}$$

This equation cannot be solved analytically for each value of v_l and v_t, but in order to fix the idea, let us suppose that the Lamè constant are equal:

$$\alpha = \beta \qquad \Rightarrow \qquad v_l^2 = 3v_t^2, \tag{1.86}$$

The numerical solution is calculated with matlab with `solve('(2-x^2)^2 -4*((1-x^2) *(1-x^2 /3))^0.5==0', 'x')` *command*

therefore the numerical solution of this equation is

$$v_R = 0.9194 v_t. \tag{1.87}$$

Putting $k_R = 1$, the quantities:

$$L = 0.8475i \qquad T = 0.3933i, \tag{1.88}$$

therefore

$$B = \frac{2k_RL}{k_R^2 - T^2}A = 1.468iA \tag{1.89}$$

and using $A = 1$ the semi-numerical solutions of displacement at $t = 0$ are

$$\begin{cases} u_{R1} = \left(e^{0.8475\cdot x_3} - 0.5774\cdot e^{0.3933\cdot x_3}\right)(\cos(x) - i\sin(x)) \\ u_{R2} = 0 \\ u_{R3} = \left(0.8475\cdot e^{0.8475\cdot x_3} - 1.468i\cdot e^{0.3933\cdot x_3}\right)(\cos(x) - i\sin(x)) \end{cases}. \tag{1.90}$$

The plot of these solutions is shown in figure (5).

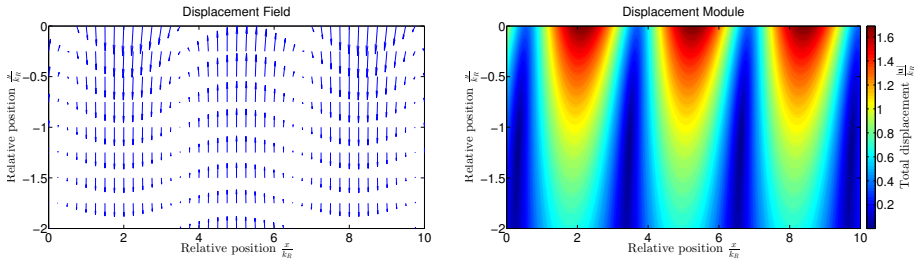

Figure 5.: *Rayleigh waves displacement field for isotropic material.*

1.4 PIEZOELECTRICITY

Following [3] and [8] we study the behavior of a solid body in an electric field: we introduce the **permittivity tensor** and the **piezoelectric tensor**, their relation through the **stress tensor**, and their most significant relations with waves propagation in crystals.

Let us consider a piezoelectric body in an electric field **E**.Its energy is

$$U = \frac{1}{2} c_{ijkl} s_{ij} s_{kl} - e_{ijk} E_i s_{jk} - \frac{1}{2} \epsilon_{ij} E_i E_j. \tag{1.91}$$

The constitutive **stress-charge** form of piezoelectric relations:

$$\begin{cases} \dfrac{\partial U}{\partial s_{ij}} = \sigma_{ij} = c_{ijkl} s_{kl} - e_{kij} E_k \\ -\dfrac{\partial U}{\partial E_i} = D_i = e_{ijk} s_{jk} + \epsilon_{ij} E_j \end{cases}, \tag{1.92}$$

or using the displacement **u** and the potential ϕ:

$$\begin{cases} \sigma_{ij} = c_{ijkl} \partial_l u_k + e_{kij} \partial_k \phi \\ D_i = -\epsilon_{ij} \partial_j \phi + e_{ijk} \partial_k u_j \end{cases}. \tag{1.93}$$

When a Rayleigh wave travels on the surface of a piezoelectric material, the mechanical perturbation is coupled with an electric field. Following [7], in principle the motion is described by the solution of both Newton and Maxwell equations. In practice the velocity of mechanical waves are 10^5 times lower than the electromagnetic ones: this means that we can use the electrostatic approximation:

$$\begin{cases} \partial_i D_i = 0 & z < 0 \\ \partial_i E_i = 0 & z > 0 \end{cases}. \tag{1.94}$$

The Newton law is given by (1.46):

$$\rho \ddot{u}_i = c_{ijkl} \partial_j \partial_l u_k + e_{kij} \partial_j \partial_k \phi. \tag{1.95}$$

As in the isotropic case the **mechanical boundary conditions** are obtained imposing a stress free surface along the z direction, but the piezoelectric equations introduce an **electric boundary condition** of continuity for **D**:

$$\begin{cases} \sigma_{i3}(x_3 = 0) = 0 \\ D_3(z = 0^+) = D_3(z = 0^-) \end{cases}. \tag{1.96}$$

These equations will be solved numerically with finite element method.

1.5 REFLECTING GRATINGS

Reflecting gratings can be studied treating each strips as a 2-port network and summing up the global behavior: this procedure is called reflective array model (RAM). We will apply this method to an array of strips an then to resonator cavities.

1.5.1 *Reflective Array Model*

Following [5], let's consider an array of stripes of width w and pitch p. A wave from the left, with amplitude c_{n-1}, hits the $n-$th electrode and continues with amplitude c_n towards the next one. Another wave from the opposite direction and amplitude b_n arrives on the $n-$th electrode and continues with amplitude b_{n-1}. Since the electrodes are all the same, their reflection coefficients are $S_{11} = r_1 \exp(-ikp)$ and $S_{22} = r_2 \exp(-ikp)$, and their transmission coefficient $S_{21} = t \exp(-ikp)$, where k is the wavenumber of the waves that hit the electrode. As we are neglecting any losses t is real, and using the equation (A.6):

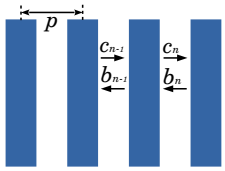

Infinite array of stripes.

$$r_1 = -r_2^*, \tag{1.97}$$

i.e. r_1 and r_2 are pure imaginary numbers, and because of the symmetry of the system $r_1 = r_2 = r$.

The amplitudes of traveling waves can be written as

$$\begin{cases} b_{n-1} = (rc_{n-1} + tb_n)\exp(-ikp) \\ c_n = (rb_n + tc_{n-1})\exp(-ikp) \end{cases}, \tag{1.98}$$

and expressing the waves on the right as function of waves on the left

$$\begin{cases} b_n = \dfrac{1}{t} b_{n-1}\exp(ikp) - \dfrac{r}{t} c_{n-1} \\ c_n = \dfrac{1}{t} c_{n-1}\exp(-ikp) + \dfrac{r}{t} b_{n-1} \end{cases}. \tag{1.99}$$

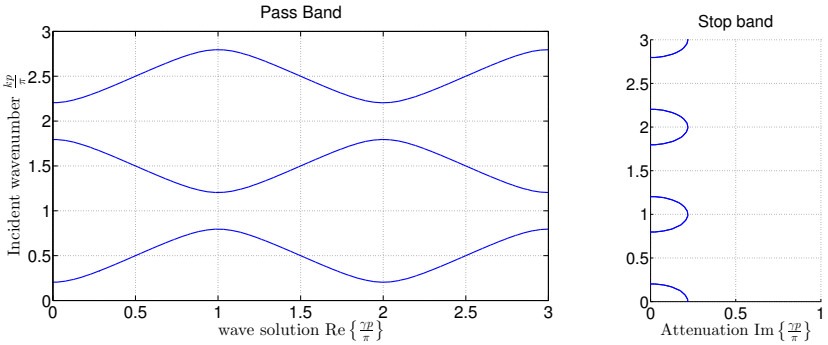

Figure 6.: *Band solutions for reflective gratings (exaggerated* $|r| = 0.2$ *in order to make the effect visible).*

Since the grating is infinite, taking the ansatz of the **Bloch waves**

$$c_n = c_{n-1}\exp(-i\gamma p) \quad \text{and} \quad b_n = b_{n-1}\exp(-i\gamma p), \tag{1.100}$$

the system reduces to equation

$$t\left[\exp(i\gamma p) - \exp(-i\gamma p)\right] = \left[\exp(ikp) - \exp(-ikp)\right], \tag{1.101}$$

that can be written as

$$\cos(\gamma p) = \frac{\cos(kp)}{t}. \tag{1.102}$$

Usually $|r| \approx 10^{-3}$ *and* $t \approx 1 - 10^{-3}$

The transmission coefficient $t \approx 1$ but is still smaller than 1. This implies that most of the incident waves frequencies pass through the grating without attenuation, and $\gamma \approx k$. When k goes near $\frac{n\pi}{p}$ the left term in equation (1.102) becomes larger than 1, therefore γ becomes imaginary, that means an attenuation of the incident waves. The limits of the **stop band** are the values of k_0 that make γ imaginary

$$\frac{\cos(k_0 p)}{t} = 1 \quad \Rightarrow \quad k_0 = \frac{1}{p}\arccos(t) = \frac{1}{p}\arcsin\left(|r|\right). \tag{1.103}$$

Because $|r| \ll 1$ we can write

$$k_0 \approx \frac{|r|}{p}, \tag{1.104}$$

therefore we have the stop band

$$\Delta k = 2\frac{|r|}{p}. \tag{1.105}$$

In order to express the stop band as a function of frequency, differentiation of $f = \frac{v}{\lambda} = \frac{v}{2\pi k}$ gives

$$\Delta f = \frac{v}{2\pi}\frac{\Delta k}{k^2} = f_0\frac{\Delta k}{k}, \tag{1.106}$$

and substitution of Δk

$$\Delta f = f_0 \cdot 2\frac{|r|}{\pi}. \tag{1.107}$$

If the array has N number of strips, using the cascade equation for S-parameters (A.16), and keeping in mind that in the stop band $\theta = \gamma p$ is imaginary:

$$\begin{aligned} S_{11} &= S_{22} = -\tan(N\gamma p) \\ S_{12} &= S_{21} = \frac{1}{\cos(N\gamma p)} \end{aligned} . \tag{1.108}$$

In the center of the stop band, the equation (1.102) becomes

$$\frac{1}{t} = \frac{1}{2}\left(e^{i\gamma p} + e^{-i\gamma p}\right), \tag{1.109}$$

and considering that $|r| \ll 1$ its solution is:

$$e^{i\gamma p} = -t \pm r \quad \Rightarrow \quad |\gamma p| \approx |r|. \tag{1.110}$$

With this approximation, the reflection coefficient for a wave in the stop band is:

$$S_{11} = -i\tanh(N|r|). \tag{1.111}$$

It can be shown [5] that r can be expressed as the combination of an electrical and a mechanical effect:

$$r = r_e + r_m = ic_1 + ic_2\frac{h}{\lambda}, \tag{1.112}$$

where c_1 and c_2 are constants that depend on the material, and h is the thickness of the metal layer.

This expression of r can be seen as the first terms of a multi-scale expansion. The order of magnitude of constant is $c_1 \sim 10^{-}3$ and $c_2 \sim 10^{-}1$.

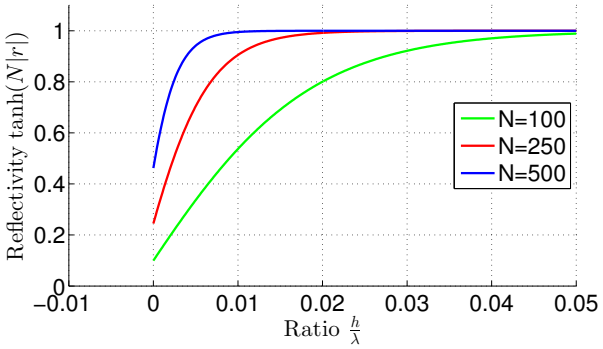

Figure 7.: *Module of the reflectivity in function of the ratio between metal thickness and wavelength for different number of strips.*

In figure 7 it is shown the module of S_{11} in function of the ratio between metal thickness and wavelength. The reflectivity of a mirror with few lines can be enlarged using a higher layer of metal.

1.5.2 *Cavities and Resonators*

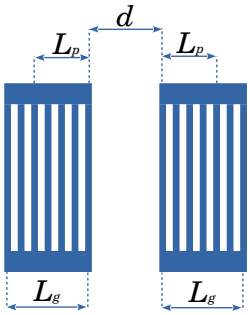

Cavity dimensions.

If two mirrors are placed one in front of the other, a SAW with the frequency in the stop band is reflected back and forward, acquiring a phase in every reflections. This face is given by (1.111) and is equal to $\phi_g = -\frac{1}{4}\pi$.

If the distance of the gratings is d (measured from the center of their first strips), when the wave completes a cycle in the cavity, it has a phase of

$$\Delta\phi = 2\phi_g + \frac{2d}{\lambda} \cdot 2\pi, \tag{1.113}$$

where the second term is the phase due to the traveling for two cavity lengths.

If this phase is an integer multiple of 2π the wave is in phase, and there is a constructive interference:

$$\Delta\phi = 2n\pi \quad \Rightarrow \quad d = \left(n + \frac{1}{2}\right)\frac{\lambda}{2}; \tag{1.114}$$

in this case the cavity is called **resonant cavity**.

The mirror works as a distributed Bragg reflector, i.e. the wave is not completely reflected in the cavity, but it presents a **penetration length** L_p in the grating. It can be shown [5] that

$$L_p = \frac{\lambda}{4|r|}, \tag{1.115}$$

and therefore we can define the total cavity length L_c:

$$L_c = d + L_c. \tag{1.116}$$

In a resonant cavity the possible modes that can be confined depend on the dimension of the cavity itself. The **central mode** of the cavity is located at the center of the stop band

$$k_0 = \frac{\pi}{p} = \frac{2\pi f_0}{v} \quad \Rightarrow \quad f_0 = \frac{2p}{v}, \tag{1.117}$$

and it is always present. When the center mode SAWs are confined in a cavity of length L_c, there are

$$n_w = \frac{L_c}{\lambda_0} = \frac{1}{2}(n + \frac{1}{2}) + \frac{1}{|r|}. \tag{1.118}$$

In order to find the **next resonant mode** we have to look for the frequency that confines in the same cavity length L_c a number of $n_w + 1$ stationary waves:

$$f_1 = f_0 + f_0\frac{\lambda_0}{L_c}. \tag{1.119}$$

If the frequency of this mode is in the stop band of the grating, this is a resonant mode of the cavity, and therefore we have a **multi-mode cavity**. Otherwise, the waves with this frequency are not reflected, and the cavity presents only the single central mode.

In order to excite these cavities we can insert and IDT in the space between the mirror, as displayed in figure 22. The distance between the mirror continues to respect the relation (1.114) and the IDT is placed symmetrically in the center. These devices are called **resonators**: their fabrication and characterization in the main task of this thesis.

2

EXPERIMENTAL SETUP

The main phases of the experiment are:

- the **design** of the device layout/mask using a CAD;
- the **fabrication** of the devices by optical lithography;
- the **bonding** of the devices to a PCB;
- the **characterization** of the devices.

The whole steps usually took 1-2 weeks. In this work we made 4 masks in which we tested filters and resonator on GaAs.

2.1 DEVICES DESIGN

Devices are designed considering both the fabrication process and the working features. The hierarchical layout editor **CleWin** gives a graphical interface with basilar shapes and layer instruments. The result is a mask that reproduces the metallic layer in the final device (compare figure 8 and 10). The mask is loaded in the computer that controls the laser writer, and converted in instructions that turn on and off the laser in a point of the substrate.

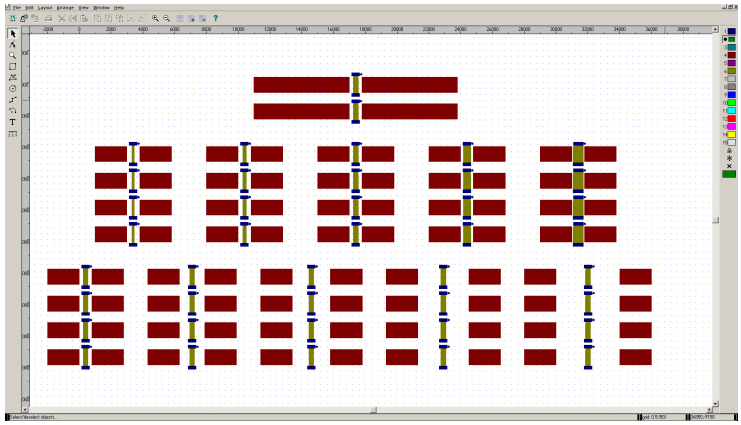

Figure 8.: *Mask designed with CleWin and realized in figure10.*

2.2 FABRICATION

All fabrication steps took place in the **clean room** (class ISO7 - 10000) of the joint laboratories among **UniSalento** and **CNR-Nanotec**.

2.2.1 *Photolithography*

GaAs wafer

Spin coating

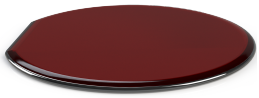

Exposure

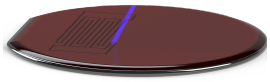

Development

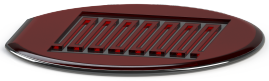

Deposition

Lift off

The process of fabrication for SAW devices is simple, because can be limited at one step of lithography, but can be tricky due to the feature of the devices.

The substrate is a GaAs wafer of 5cm of diameter and 350µm of thickness. Due to its dimensions it is very fragile, and an excessive pressure from the tweezers could break it. Moreover the steel is harder than the GaAs, therefore a considerable care is necessary in handling the wafer, trying to not scratch the surface, picking the wafer only at the edge. The crystallographic direction [110] is marked by a long cut on the wafer edge; a smaller cut is present on the perpendicular direction [−110].

The fabrication on GaAs wafer is composed by the following steps:

- **GaAs Wafer Preparation**: the wafer was placed in a 70°C **acetone** bath for 3 minutes and then washed with **isopropanol**, dried with a nitrogen gun and placed on a spinner.
- **Spin coating**: few droplets of **primer** solution (hexamethyldisilazane, HMDS) was placed on the wafer surface; the spinner worked at 300 rpm for 5 seconds and at 4000 rpm for 40s. The positive photoresist **S1805** was dropped on the wafer until the surface was completely covered, then it was spinned at 300 rpm for 5s and 4000 rpm for 40s. This produced a thin layer of resist of **600 nm** on the wafer center. Then a backing at 110°C for 2 minutes was carried out.
- **Exposure**: the wafer was placed on the moving plate of **laser writer** machine. A CAD layout previously loaded on the system was written by a laser with 400nm wavelength. The procedure takes some hours because it is sequential.
- **Development**: the exposed resist became soluble within the **development solution** (tetramethylammonium hydroxide, TMAOH). Depending on the feature of the lithography and the substrate material, this step takes between 45s and 2 minutes (larger parts are more soluble, and different substrates

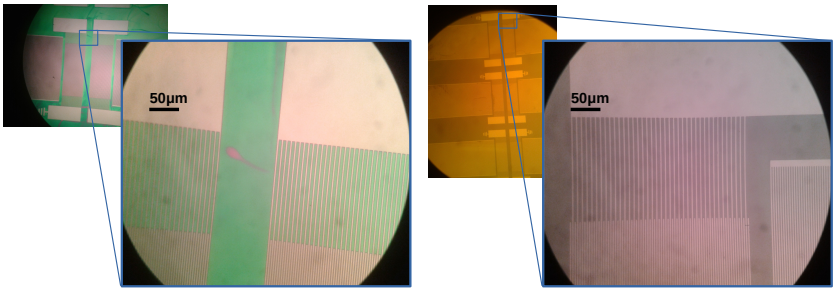

Figure 9.: *Litography steps on GaAs checked by optical microscope, development on the left and lift off on the right.*

have a different behavior). The design is checked under an **optical microscope** in order to verify that the features are well defined. If the number of defects is high, the wafer is placed in acetone that removes the resist, and the process can be repeated from the beginning.

- **Deposition**: the wafer was placed in a **metal evaporator** where a thin layer (50 or 100 nm depending on the mask) of **aluminum** was deposited on the wafer surface.

- **Lift Off**: the wafer was placed in a 70°C **acetone** bath for 5 minutes, and if necessary ultrasounds were applied. The resist is soluble in acetone and the metal on it was removed in this step. The wafer was inspected under the optical microscope in order to check for small part of resist that remains on the wafer.

In figure 9 the results of a photolithography process is shown, in particular the fabrication of SAW resonators on GaAs. Each finger is 2µm wide and 1000µm long. In figure 10 the wafer is shown with all devices on it. Notice the **edge effect** that causes the loss of the outer devices.

The lithography process on GaN heterostructure on Sapphire has the same steps, but there are some differences in the used parameters. We noted that the resist presents a lower adhesion on GaN; on the other hand the metal adhesion is better than the one on GaAs, and more ultrasounds were necessary to clean the samples.

2.2.2 *Wafer Dicing*

The photolithography process produces a wafer with a large number of devices on it. To measure each devices it is necessary

to separate them in small pieces that fit in the PCB housing (about 5x5 mm^2).

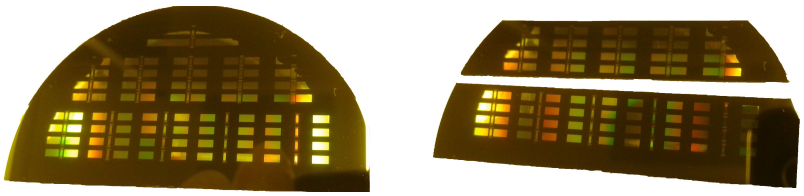

Figure 10.: *Dicing process of GaAs wafer, after the lift off.*

Since the GaAs is less hard than the steal, it is sufficient to incise with a **scalpel** the substrate along a crystallographic direction. The scalpel produces less debris with respect to a **spearhead**. After the incision, a little pressure with the tweezers on the surface is enough to cut the wafer.

2.2.3 *Fabrication Issues*

Resist edge effect on half wafer.

The particular geometry of our SAW devices requires strong attention to each step of the fabrication. The main problems are of two kinds: the **aspect ratio** and **repetition**. Each finger is about 1000 times longer than wide; in a usual device there are about 1000 repetitions of these fingers. This means that the device usually has a large extension compared with its smaller features. Therefore it is clear that the resist must have a uniform height.

When the wafer spins, the resist on its top is affected by defects. The edge itself is a defect so that the resist does not have the same height there: this effect is enhanced if the edge is sharp. Due to interference it is possible to see where the resist has different thickness, because different colors are visible on the wafer. At the end of the fabrication process the edge effect on the resist appears as an edge on the devices (see figure 10).

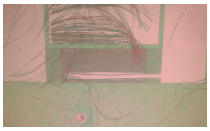

Resist adhesion problem .

Another issue is due to the resist adhesion on the substrate. Since some device features, like the mirrors in the resonators, leave long thin resist strips of resist, if the sample is not perfectly clean, or its surface presents some defects, the resist can just fall off during the development.

2.3 BONDING

After the fabrication, we end up with a series of 5x5 mm^2 pieces of GaAs substrate, with SAW devices on them. In figure 11 a printed circuit board (PCB) is shown for radio frequency application; it is composed of a dielectric base with three electrodes per each side.

Two SMA (SubMiniature version A) connectors are soldered to the PCB. An insulator stripe of adhesive material is placed on the center of the PCB, and the sample is placed on it.

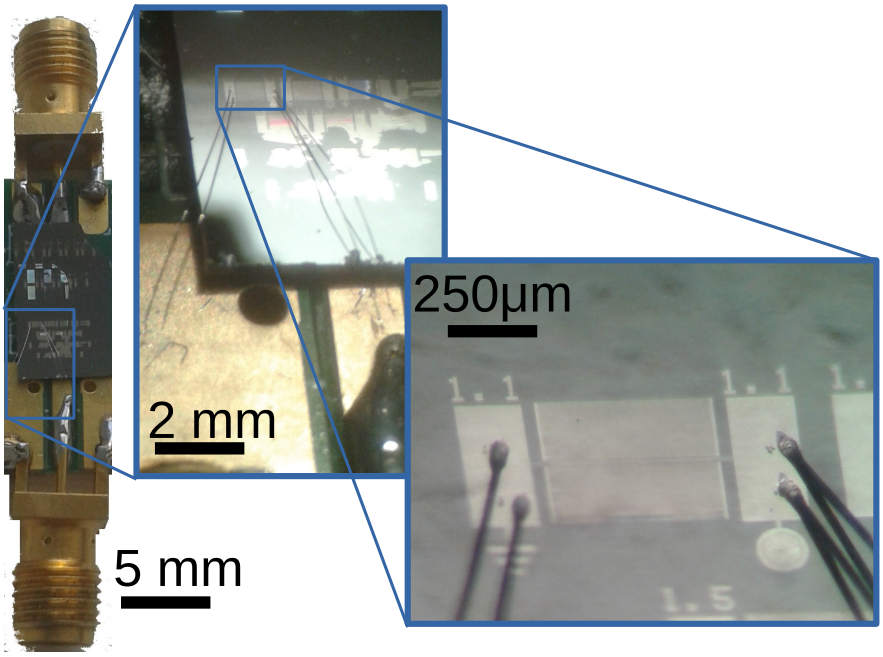

Figure 11.: *Single devices mounted on the PCB and bonded.*

The sample is electrically connected to the PCB with Ø25µm aluminum wires soldered with ultrasounds. If the bond pad on the sample is large enough a good practice is to bond more than one wire per electrode; in fact sometimes the wire is actually just resting on the sample metal layer. The **bonder machine** consists of a holed tip, in which the wire goes, and the clips that handle the wire. The ultrasonic vibration of the tip, that squeezes the wire against the bond pad, bonds the wire.

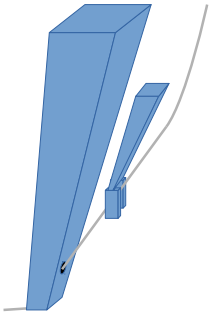

Tip and Clip of the bonder machine.

The machine setting consists of three parameters: the force that the tip produces on the substrate, the time of the application of the ultrasounds, and the power, i.e. the amplitude of oscillation of the tip. The metal, the metal thickness, the substrate, all influence the bonding, and the correct parameters need to be searched every time these conditions change.

2.4 INTRUMENTS SETTING

2.4.1 *Spectrum Measurements*

In figure 12 the experimental set up for the spectrum measurements of SAW devices is displayed. The USB port of a laptop is

connected to the serial port of a **signal generator** (Agilent MXG N5183A) and a **spectrum analyzer** (Agilent MXA N9010). An high frequency coaxial cable connects the signal generator to a SMA connector on a PCB side. The other side is connected through another coaxial cable to the spectrum analyzer.

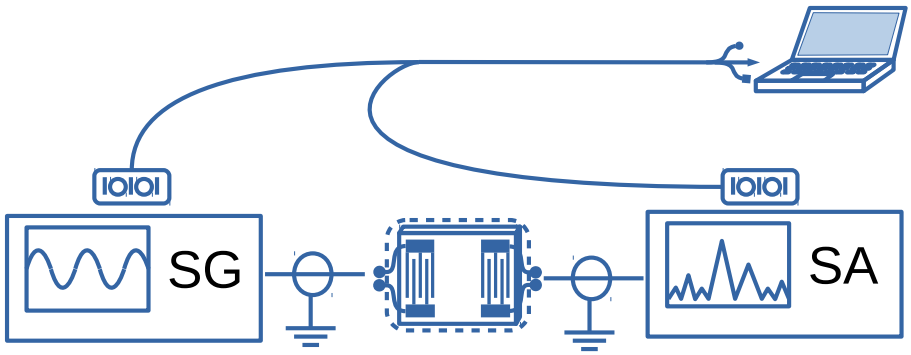

Figure 12.: *The software* LABVIEW *installed on a laptop controls the signal generator (SG) and the spectrum analyzer (SA).*

The instrument settings are controlled by a LABVIEW program written by prof. Maruccio. In the dialog window of the program the frequency range and the number of points are set; the amplitude of signal is manually chosen on signal generator. The program spans setted frequency range collecting the amplitude of the signal that arrives to the spectrum analyzer.

In the reflection measurements a **directional coupler** (Mini-circuits ZEDC-15-2B) is placed in the position of the sample as shown in figure 12, between the signal generator and the spectrum analyzer, and the sample is connected to the input of the directional coupler.

2.4.2 *Time Resolved Measurements*

The time resolved data are collected using the set up shown in figure 13. A **pulser** (Agilent 81 11 0A) is connected using a coaxial cable to the trigger of the signal generator. Another coaxial cable connects the generator to the PCB where is the sample, and an oscilloscope (Agilent DSO-X 3052A) is placed at the other side of the PCB.

The pulse setting are manually chosen on the pulser control panel: the parameters are pulse **amplitude** (always set at 1 Volt because is used just to trigger the signal generator), pulse **width**,i.e. the time extension of the pulse, and the pulse **period**, i.e. time with which the pulse are repeated. The generator is manually set,

choosing the signal amplitude and frequency. The measures are loaded from the oscilloscope on a USB storage drive.

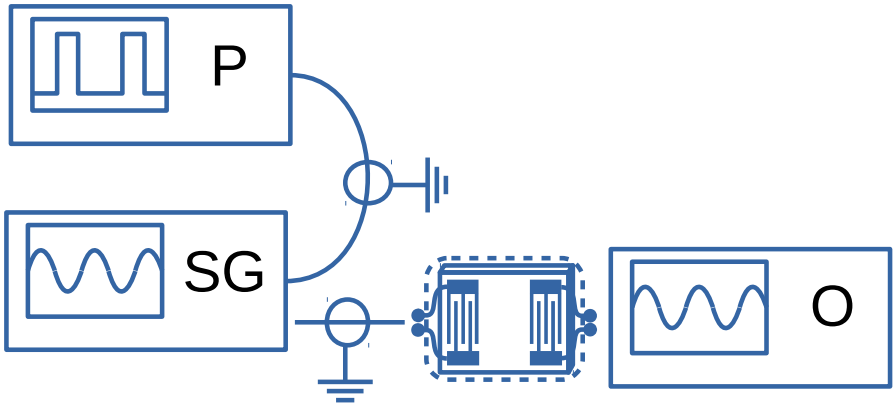

Figure 13.: *A pulser (P) triggers the signal emitted by the signal generator (SG) and an oscilloscope (O) reads the measures.*

As mentioned before, the set up for the reflection measurements is the same, except for the use of a directional coupler.

3

MEASUREMENTS AND RESULTS

3.1 SAW FILTERS

In this section the measurements on SAW filters are shown and different filters geometry features is tested.

3.1.1 *Filter Spectrum*

A typical spectrum of a SAW filter is shown in figure 14: the resonance of the device is clearly visible in a very narrow frequency range, and the peak of the signal is about 2 order of magnitude larger than the background. The background trend is due to the electromagnetic signal since an IDT works as an antenna as well as an electromechanical transducer.

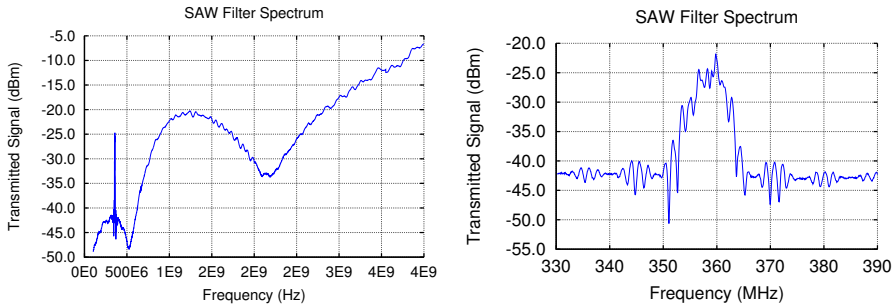

Figure 14.: *Spectrum of a SAW filter with IDT of 40 pairs of 2 µm on GaAS with an input of 10 dBm.*

In the plot of the zoom of the resonance we see the central peak with a bandwidth of about 15 MHz, in accordance with (1.31). The ground offset is around -42 dBm, which is higher than the electromagnetic noise that for this instrument is -70 dBm: this is due to the electromagnetic transmission between the two IDT, as we will see in figure 19 that shows the same device of figure 14 measured in time domain.

3.1.2 *Filter on GaAs*

The first mask designed contained the devices presented in table 1. These devices have been realized in order to investigate which

n_p	d (μm)	Geometry
40	102	single
40	1502	single
40	1502	double
80	502	single
80	502	double
120	102	single
120	502	single
120	502	double

Table 1.: *Devices of the filters comparative mask on GaAs. The metal layer is* 50nm *of Aluminum.*

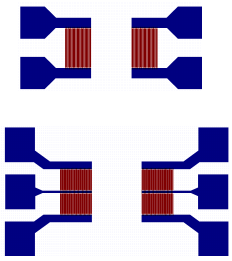

Respectively single and double geometry for SAW filters.

are the best features for SAW filters; although in principle the theory of SAW devices is well developed, this preliminary study is useful in order to understand the optimal characteristics to use in the following design of resonators and probe the increasing difficulties in fabrication when increasing the number of fingers.

Figure 15 shows the comparison between different geometries (single and double) changing the number of pairs. Independently on the geometry, the bandwidth is proportional to $\frac{1}{n_p}$, going from about 15MHz for devices with 40 IDT pairs, to about 10 MHz for filter with 80 IDT pairs, till about 5 MHz for IDT composed by 120 pairs, as expected from equation (1.31).

Another geometry-independent feature is the increasing of the transmission coefficient S_{12} at the resonance frequency, with the number of pairs. For the device with 40 pairs $S_{12} \approx -32$dB for both simple and double geometry, for $n_p = 80$ the transmission coefficient $S_{12} \approx -23$dB, and finally for IDT with 120 pairs we measured $S_{12} \approx -20$dB. This means that the transmitted power increases about one order of magnitude going from 40 to 80 pairs, but only doubles going from 80 to 120 pairs.

An important remark regards the ground of signals for the different geometry: the electromagnetic noise is always higher for the double geometry, regardless of the distance of IDT or the number of pairs. For this reason in the following masks we decided to use only the single geometry.

In figure 16 two couples of identical devices except for the IDT distance are compared. As noticed from the previous comparison the filter bandwidth is independent on IDT distance.

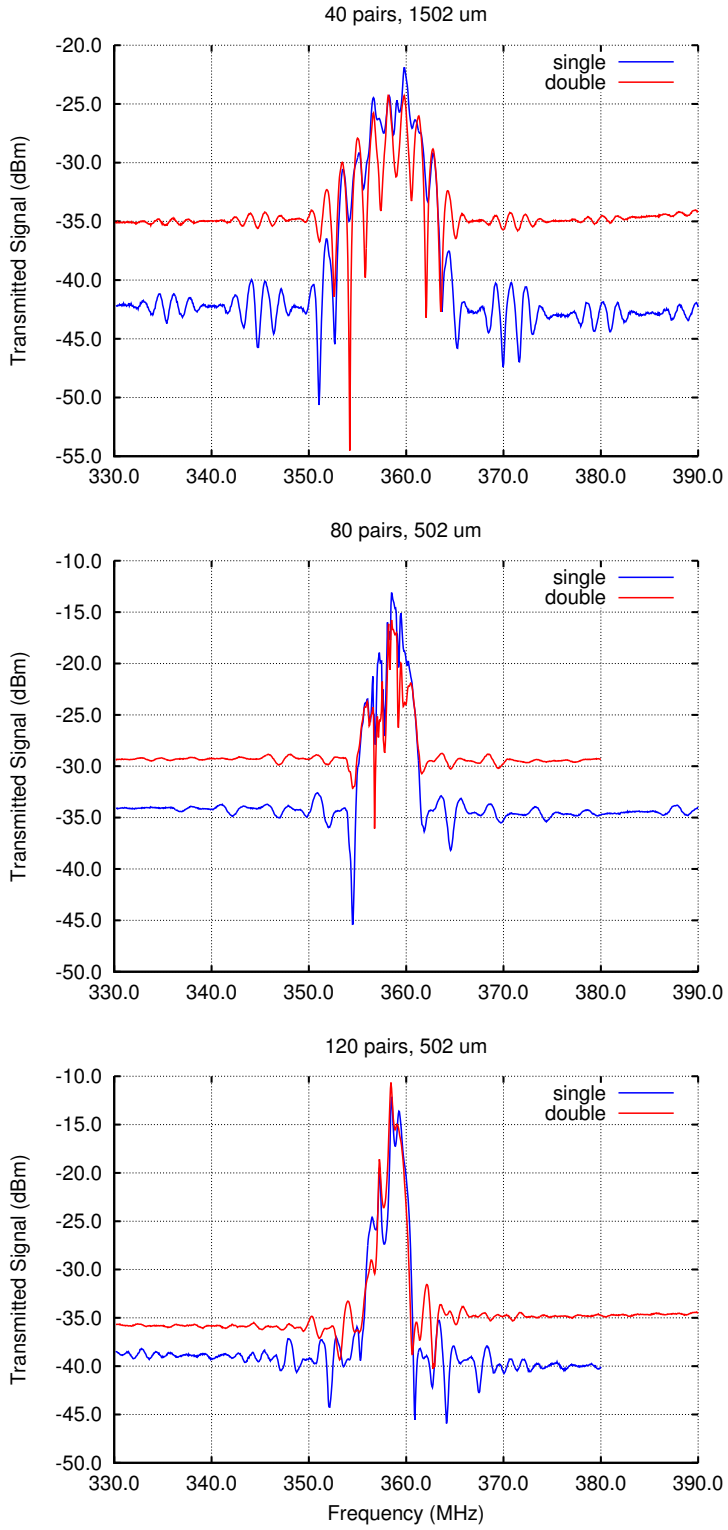

Figure 15.: *Comparison of filter with different geometry (input of 10 dBm).*

As expected, the peak of transmitted signal is slightly higher when the emitter and the receiver are closer: this can be related to

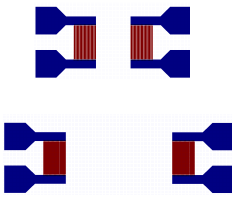

Single geometry filters with different distances between emitter and receiver IDTs.

different sources of energy losses. They can have both electrical and mechanical nature. The former are related to free charges present in the substrate (in principle this effect can be reduced cooling down the sample), the latter effect depends on two different causes: an intrinsic material loss, due to a viscosity in the shear movements, that is a second order process in the equations of motion, but can become relevant for long distances, and an external loss due to the dust deposited on the free surface, and the air above the filter.

Finally, the electromagnetic noise is lower when the IDT are placed farther away. This effect is evident if we consider that the electromagnetic wavelength is around 1m (in vacuum): the IDTs work as antennas in the near field, and the transmitted power decrease exponentially with the distance.

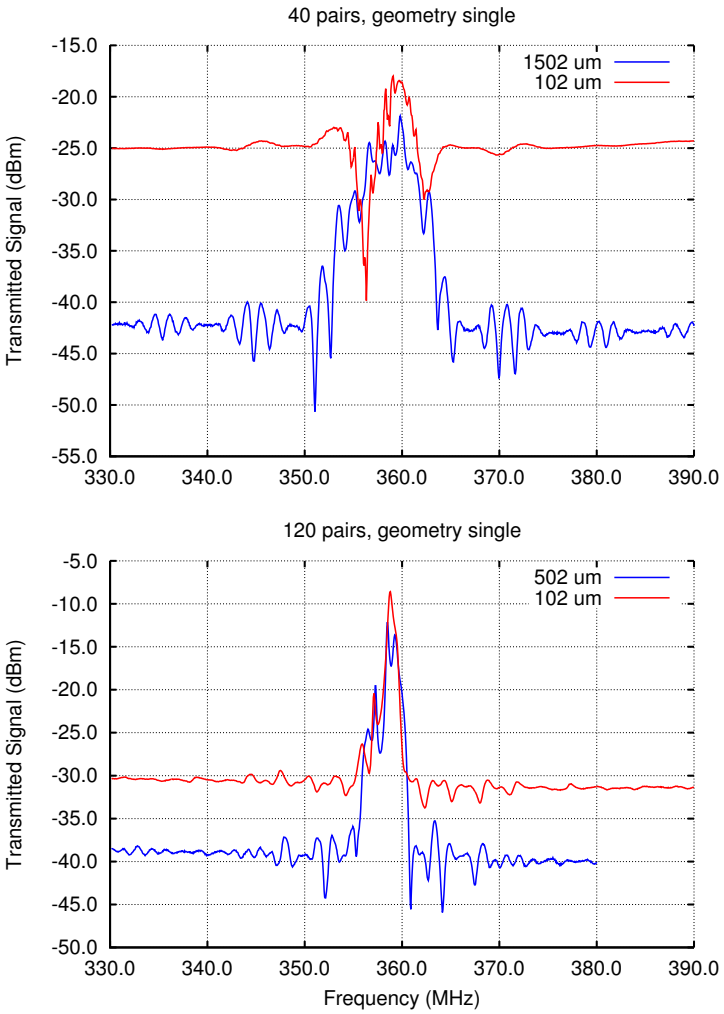

Figure 16.: *Comparison of filter with different distance between emitter and receiver (input of 10 dBm).*

Figure 17 compares similar devices with different number of pairs. As we already observed, almost always the higher of number of finger pairs the stronger the transmitted signal.

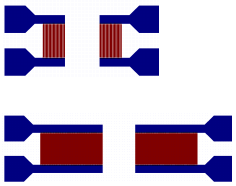

Single geometry filters with different number of IDT pairs.

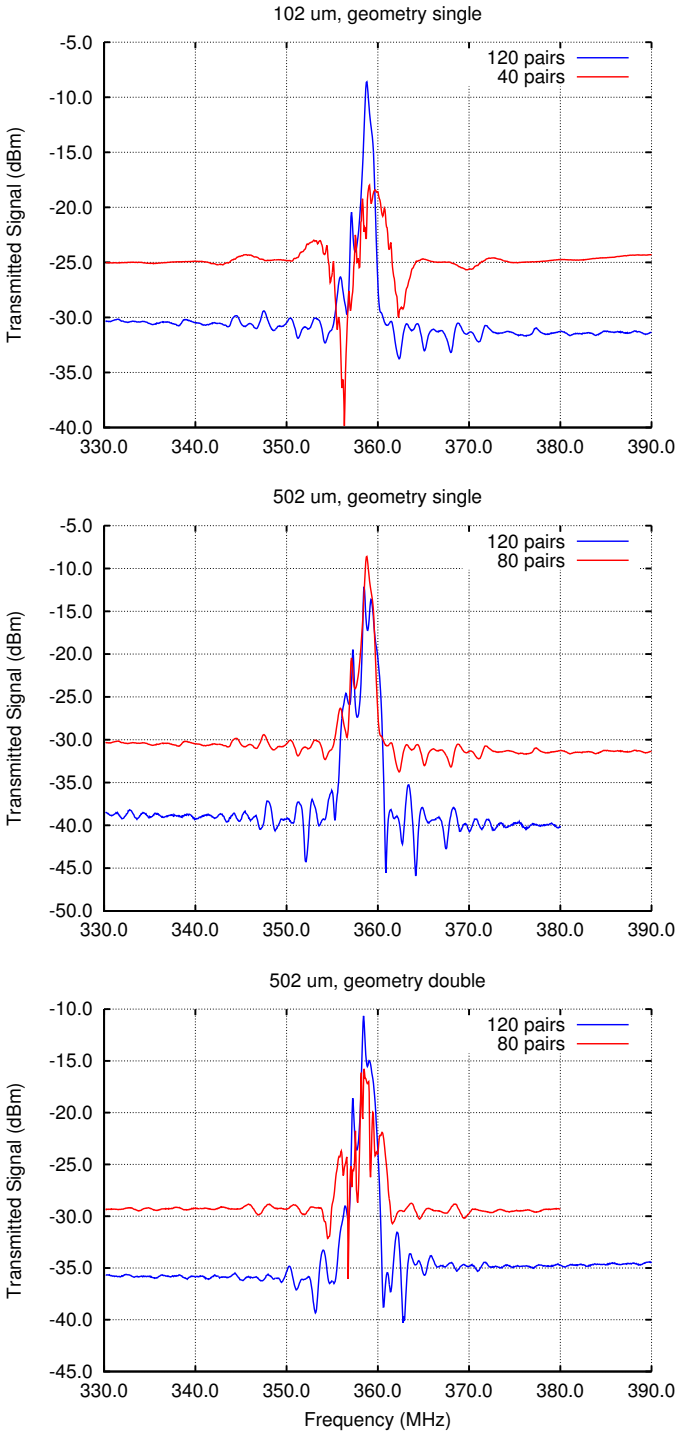

Figure 17.: *Comparison of filter with different number of pairs in the IDT (input of 10 dBm).*

3.1.3 *Impulse Measurements*

An IDT launches the mechanical wave as soon as an oscillating potential is applied to the electrodes at the resonance frequency . If this potential is placed for a short amount of time, and the two transducers are far enough, an impulse of SAW can travel in the space between the two IDT, as shown in figure 3. Using an oscilloscope connected to the receiver IDT, it is possible to detect and distinguish the mechanical and the electromagnetic impulses thanks to their different propagation velocity. The raw data from the oscilloscope is presented in figure 18.

The device used in this picture has IDT composed by 40 pairs of fingers, and the distance between the two IDT is $d = 1500\mu m$. A pulse signal of 200ns modulated by an harmonic signal of frequency 360MHz actives the first IDT, generating **a mechanical and an electromagnetic pulses** composed by 72 oscillations. The electromagnetic signal travels at the speed of light in the air, therefore it takes about $5 \cdot 10^{-3}$ns to reach the receiver: this impulse is visible in the extreme right of figure 18. The SAW signal has instead a velocity of $2860\frac{m}{s}$ along the [110] GaAs direction, therefore it takes about 600ns to cover the distance d. Its shape is due to the **constructive effect**: the deformation produced by the first pair of fingers travels to the next pair and, if the frequency is the right one (resonance condition), it arrives there in phase with the new electrical signal which then enhances this deformation. The maximum deformation is reached when summing a constructive contribution from all the n_p pairs in the array (40 in this case), which corresponds to the central part of wavepacket. Otherwise, at the beginning of the pulse generation, the waves originated by the IDT pair closest to the receiver do not undergo to this process (or undergo it to a smaller extent). Similarly, when the pulsed signal is turned off, the waves starting from the fingers farthest from the receiver will travel in a inactive IDT without receiving any amplification. The pulse is therefore composed by waves with a crescent amplitude until a maximum is reached after a n_p number of oscillations, and then by waves with decreasing amplitude after the pulse is switched off.

Finally the receiver IDT has a tiny reflection coefficient; the same is true for the emitter one. This implies that the wave pulse is partially reflected by the IDT, back to the emitter, and then reflected again to the receiver: this phenomenon is called **triple transit**, and is visible as the third peak in figure 18.

Since we are interested in the amplitude of the signal, the **envelope** of the raw data was calculated using the module of

the **analytical signal**: calling $H(x_n)$ the Hilbert transform of the series of data x_n, the analytical signal is defined as

`abs(hilbert(x))` *in matlab.*

$$y_n = x_n + iH(x_n). \tag{3.1}$$

`smooth(x,30))` *in matlab.*

Moreover in order to make the triple transit more evident, the envelope data have been converted in a logarithmic scale, and the resulting data have been smoothed using a **moving average**, i.e. each point has been substituted with the average of its 30 nearest points.

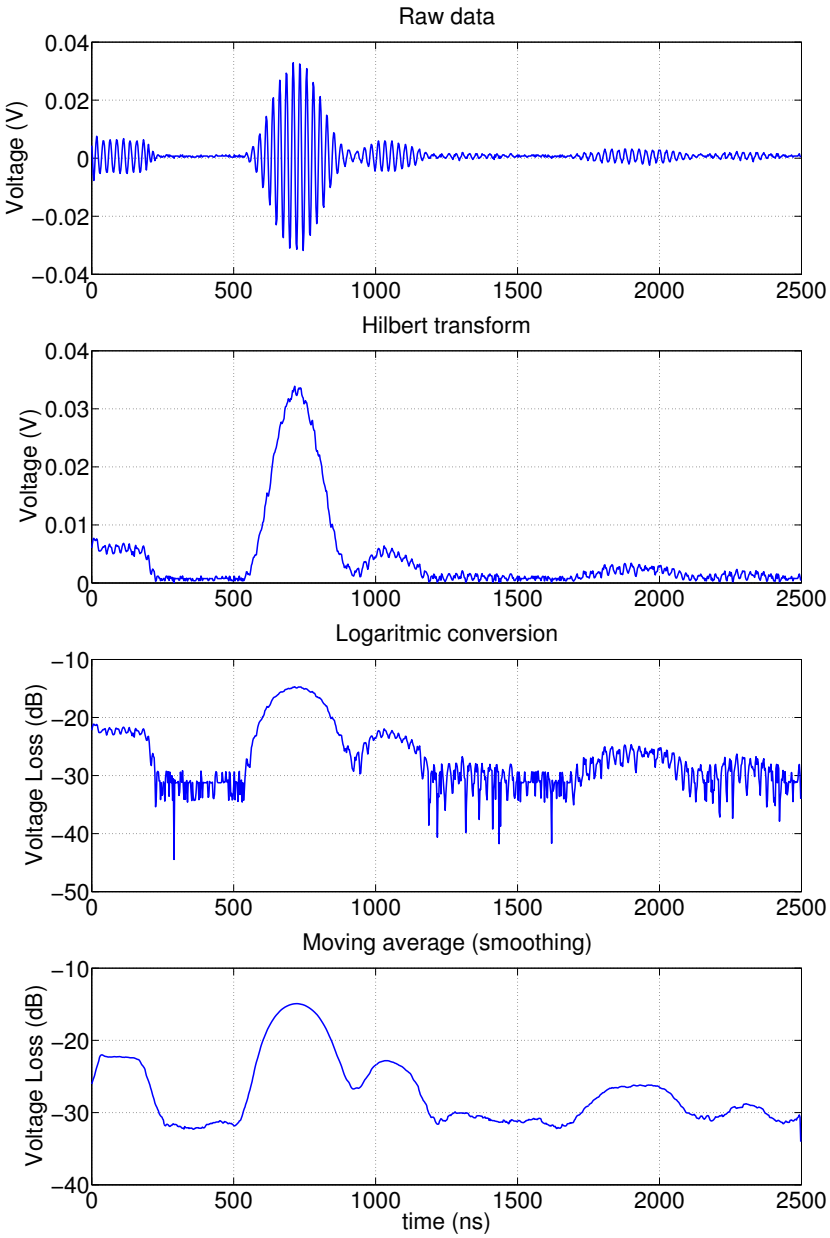

Figure 18.: *Data processing for 200 ns impulse measurements of SAW filter with IDT of 40 pairs distant 1500μm.*

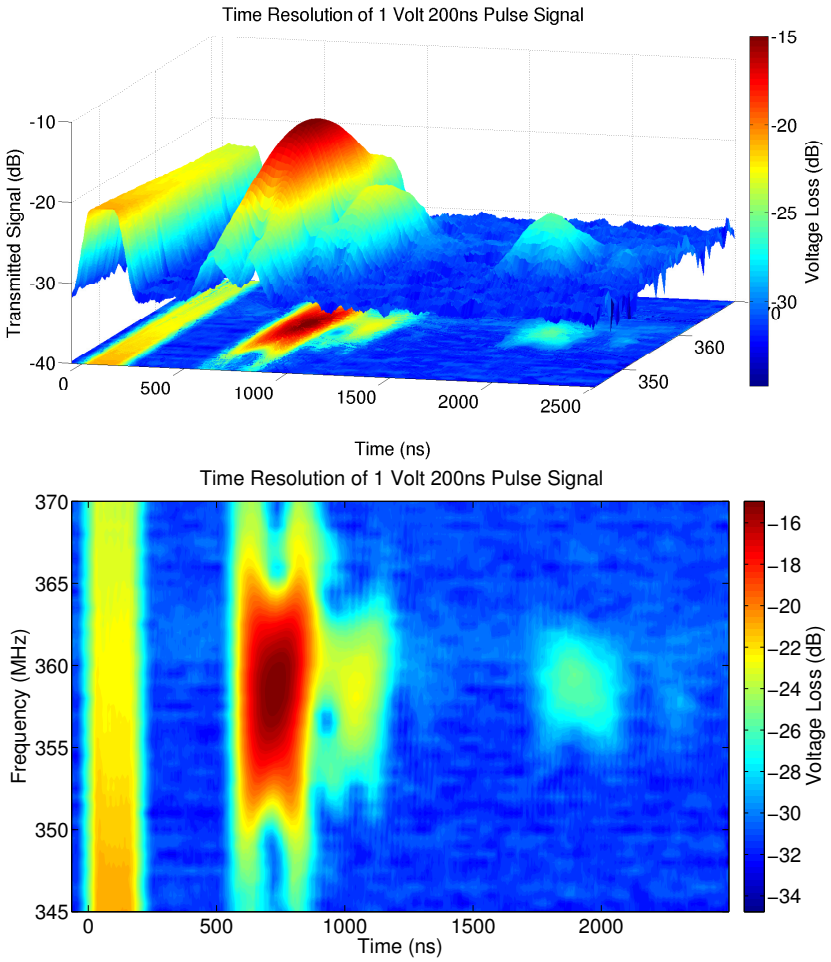

Figure 19.: *1Volt 200 ns impulse excitation ofSAW filter with IDT of 40 pairs distant 1500µm. The triple transit is visible only for resonance frequency.*

Repeating the whole procedure for different frequencies, it is possible to collect all data in a single plot, as shown in figure 19. All these operations have been automatized in a **matlab script** reported in the appendix B. It is clear how the electromagnetic signal is transmitted equally for each frequency; around 300MHz the electromagnetic wavelength is $\lambda \sim 1m$, therefore any type of constructive effect is impossible. On the other hand, the mechanical signal is transmitted only for microwave frequencies within the IDT bandwidth, already explained in figure 14. The triple transit is visible just for a further smaller range of frequencies.

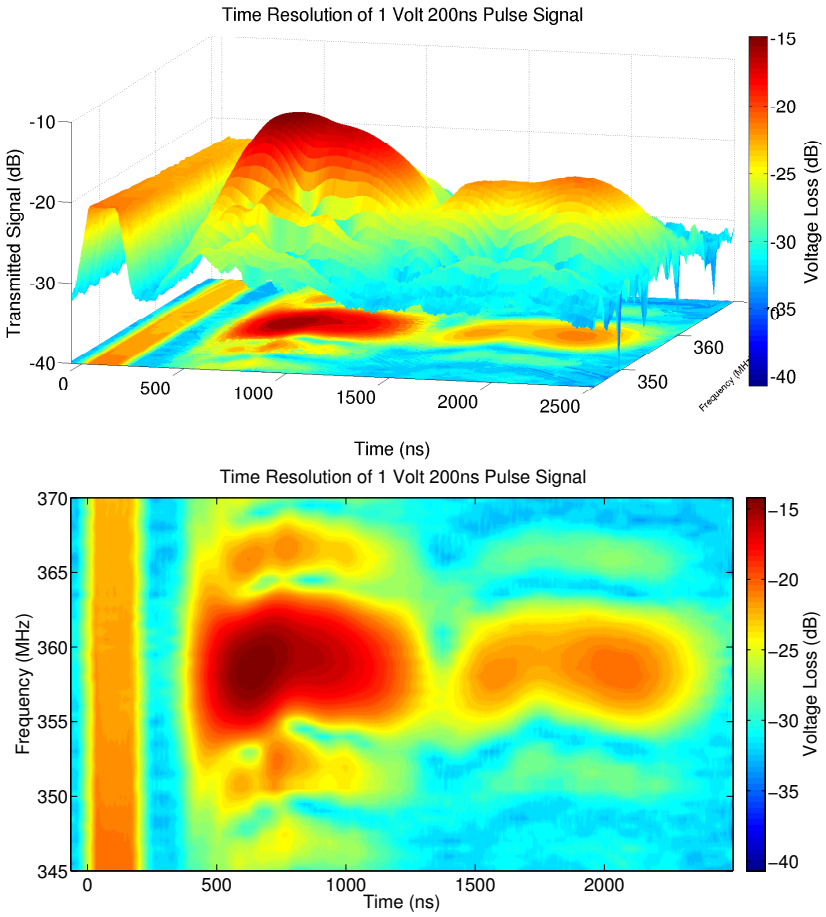

Figure 20.: *1Volt 200 ns impulse excitation ofSAW filter with IDT of 120 pairs distant 500µm.*

In figure 20 a filter is shown with IDT composed by 120 pairs of fingers, and with distance between emitter and receiver of $d = 500\mu m$. The only difference with device used in figure 19 is the number of finger pairs and the IDTs distance. As we can see the temporal extension of principal SAW signal, and the triple transit is much larger than the previous one: this is due to the physical dimension of the device. The emitter IDT is $120 \cdot 8\mu m = 960\mu m$, and the total pulse is therefore $1500\mu m$, or in temporal dimension is 600ns.

It is evident that the filter bandwidth is smaller than in figure 19 in agreement with the equation 1.31.

As expected, the triple transit signal is higher then the filter with 40 fingers, because the reflection is performed by 240 finger instead of 80.

3.2 RESONATORS

3.2.1 *Resonators Spectrum*

The spectrum of a SAW resonator is shown in figure 21: a really narrow deep of about -10dB is visible over the reflected signal. Its bandwidth is about 200kHz, and the slight asymmetry is due to fabrications defects.

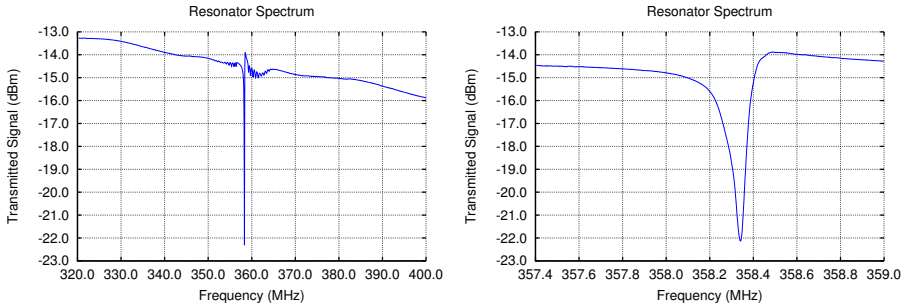

Figure 21.: *Spectrum of resonator with* $n_g = 500$, $n_p = 40$ *on GaAs. Input signal of 10 dBm.*

This kind of devices has only one port, and the reflected signal is measured with a **directional coupler**.

3.2.2 *Resonators on GaAs*

The design dimensions of a resonator are displayed in figure 22: d is the distance between the mirrors taken from the center of the fist strip, l is the dimension of the active region that emits the SAW, g is the gap between the wave front and the end of mirror, n_p is the number of pairs in the emitter and n_g is the number of electrodes in each gratings.

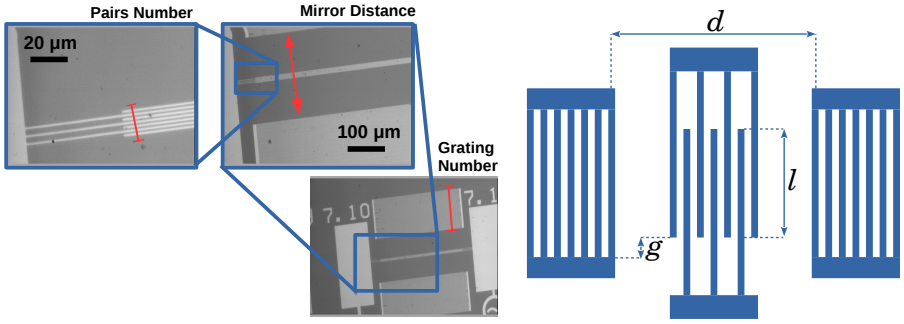

Figure 22.: *Distances used in the design of the resonators.*

The first mask for resonator contained the devices in table 2. Because the reflectivity increases with the ratio between metal

thickness and wavelength, initially we decided to make devices with finger width $w = 1\mu m$ and thicknes 50nm (made out of alluminum).

n_g	d (λ)	n_p	l (λ)	g (λ)
100	5.25	2	125	2.5
100	5.25	4	125	2.5
100	15.25	4	125	2.5
100	55.25	4	125	2.5
250	5.25	4	125	2.5
250	15.25	4	125	2.5

Table 2.: *Devices of resonator comparative mask on GaAs. The metal layer is 50nm of Aluminum.*

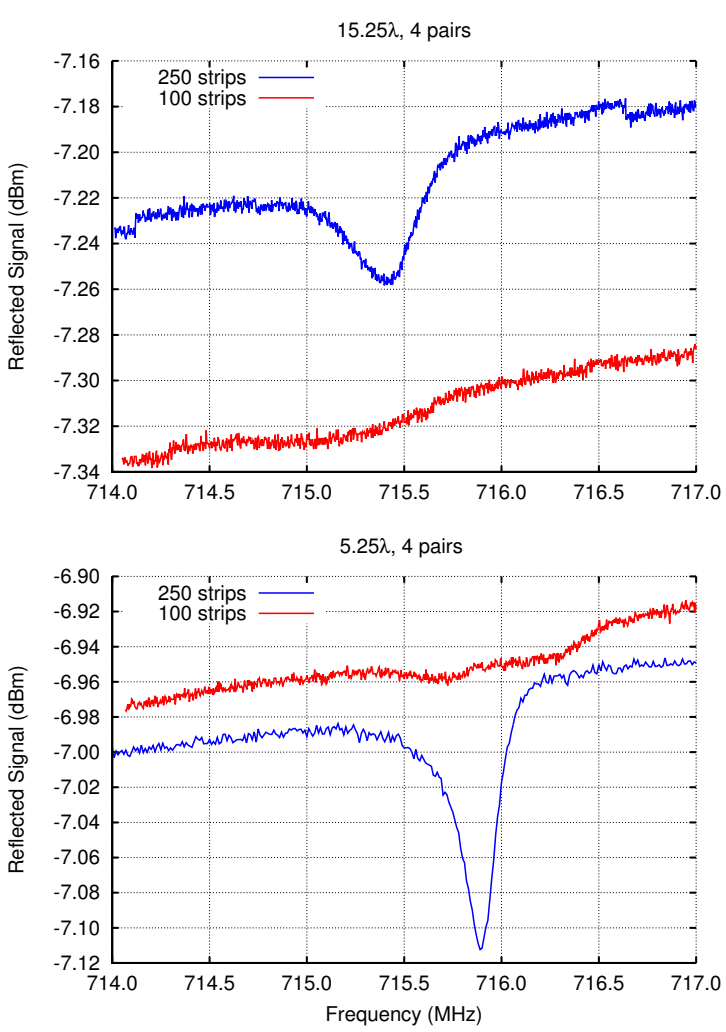

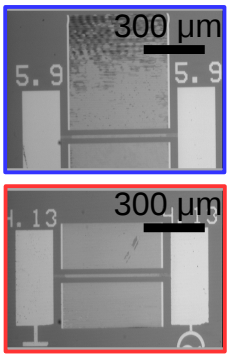

Resonator with d = 15.25λ.

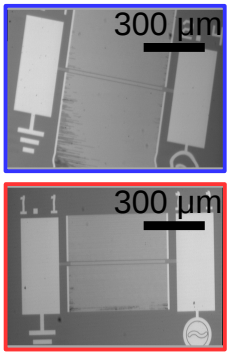

Resonator with d = 5.25λ.

Figure 23.: *Comparison between different n_g for resonators on GaAs with emitter IDT of 4 pairs, cavity l of 5.25λ and 15.25λ.Input signal 10dBm.*

Figure 23 displays the comparison between similar devices with different number of strips n_g in the mirror. Independently of the cavity dimension l and of the grating number n_g, the signal is tiny, hardly visible for the devices with $n_g = 100$ (red curve). This is due to the low number of IDT pairs, 4 for these resonators, that are not able collect enough current.

The amplitude of the signal makes difficult an accurate estimation of the Q-factor

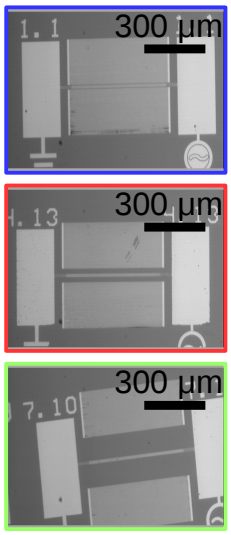

Resonator with $n_g = 100$.

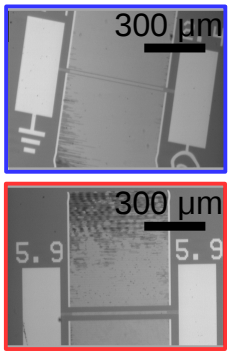

Resonator with $n_g = 250$.

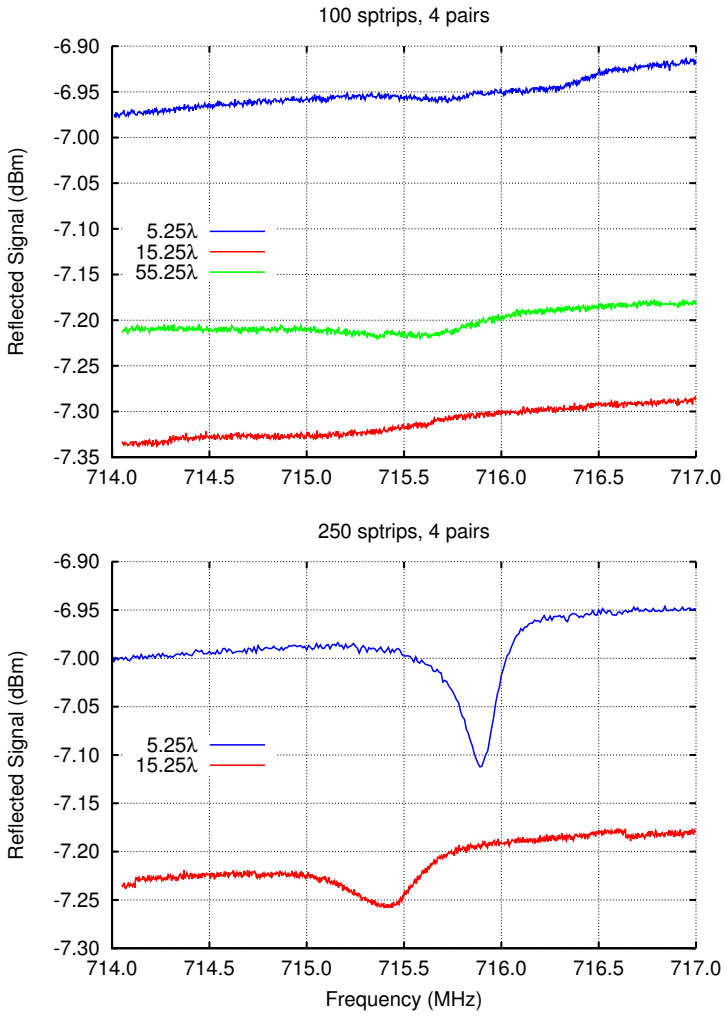

Figure 24.: *Comparison between different mirror distance for resonators on GaAs with emitter IDT of 4 pairs, mirror grating of 100 and 250. Input signal 10dBm.*

Figure 24 shows the comparison between two different cavity lengths. As said before, the data for the resonator with the mirrors composed by 100 lines is just above the noise level. Regarding the other two resonators, it seems that the smaller the cavity, the higer the signal comimng from the device (but we have to consider that

the mirrors of the resonator with $d = 15.25\lambda$ were not very clean, with some residues from the lift off on them).

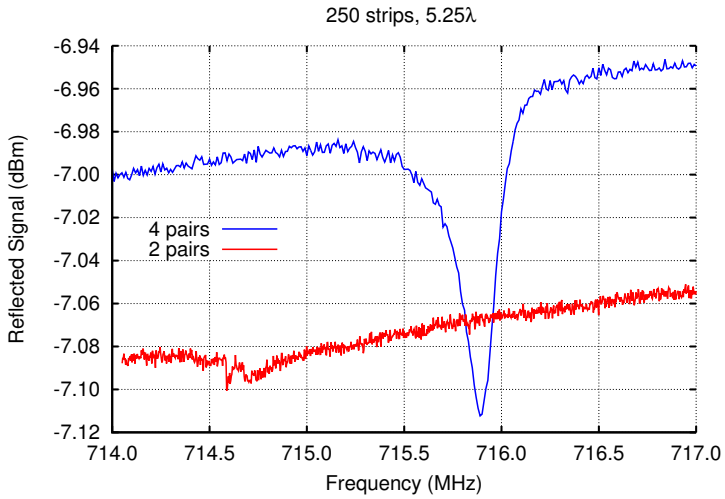

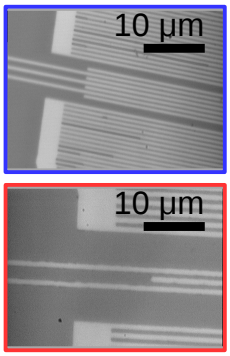

Resonator with $n_g = 250$.

Figure 25.: *Comparison between different number of pairs in the IDT for resonators on GaAs with mirror grating of 250 and a cavity of* 5.25λ. *Input signal 10dBm.*

In order to make the lift-off easier with the second mask, we decided to use $w2\mu m$ and the thickness of metal layer $h = 60nm$. The list of devices is presented in table 3.

n_g	d (λ)	n_p	l (λ)	g (λ)
250	41.25	40	31.25	1.25
500	21.25	20	31.25	1.25
500	41.25	40	31.25	1.25

Table 3.: *Resonators comparative mask on GaAs. The metal layer is* $60nm$ *of Aluminum.*

n_g	d (λ)	n_p	l (λ)	g (λ)
500	41.25	40	100	8
500	101.25	40	100	8
500	301.25	40	100	8

Table 4.: *Resonators comparative mask on GaAs. The metal layer is* $100nm$ *of Aluminum.*

The devices became very large, therefore we reduce IDT length to 33λ. Even if this could turn in diffraction problems, this reduction allows to fabricate a larger number of devices per mask.

Figure 26 shows a comparison between two resonators with 250 lines and 500 lines respectively. Comparing with figure 23, it is remarkable how the signal amplitude increases of about 2 order of magnitude. This comparison makes clear that with 500 lines grating the reflection coefficient of the mirror is much higher; in fact the enhancement due to the constructive effect produce a larger signal. Moreover the bandwidth of the resonator with 250 lines mirror is broader.

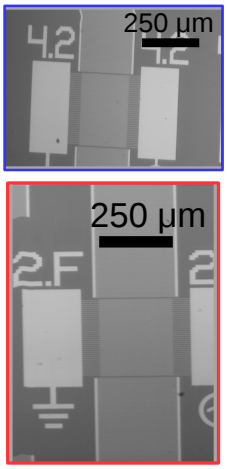

Resonator with $n_p = 40$.

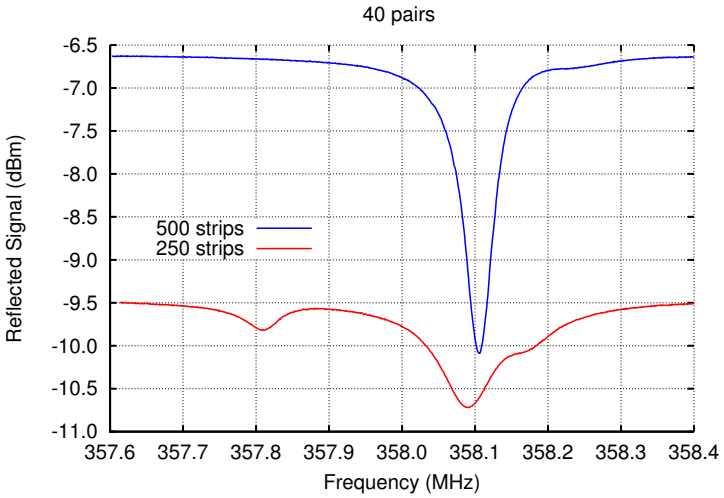

Figure 26.: *Comparison between different number of strips in the mirrors for resonators on GaAs with IDT of 40 pairs. Input signal 10dBm.*

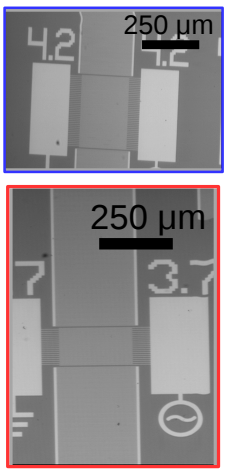

Resonator with $n_g = 500$.

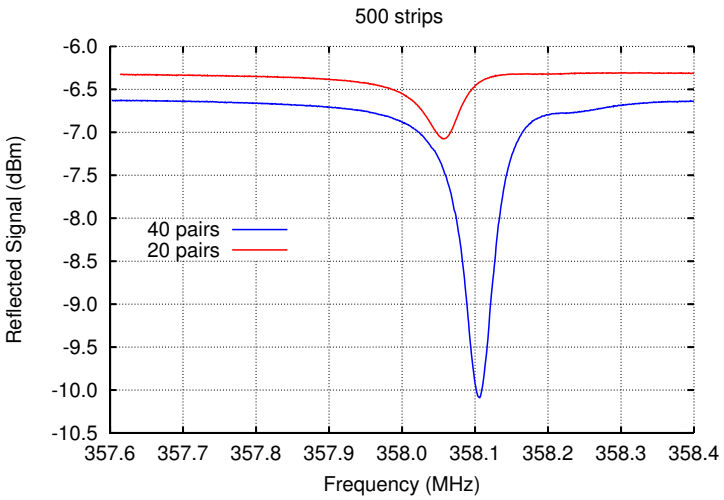

Figure 27.: *Comparison between different number of pairs in the IDT for resonators on GaAs with mirror of 500 lines and a cavity of* 41.25λ. *Input signal 10dBm.*

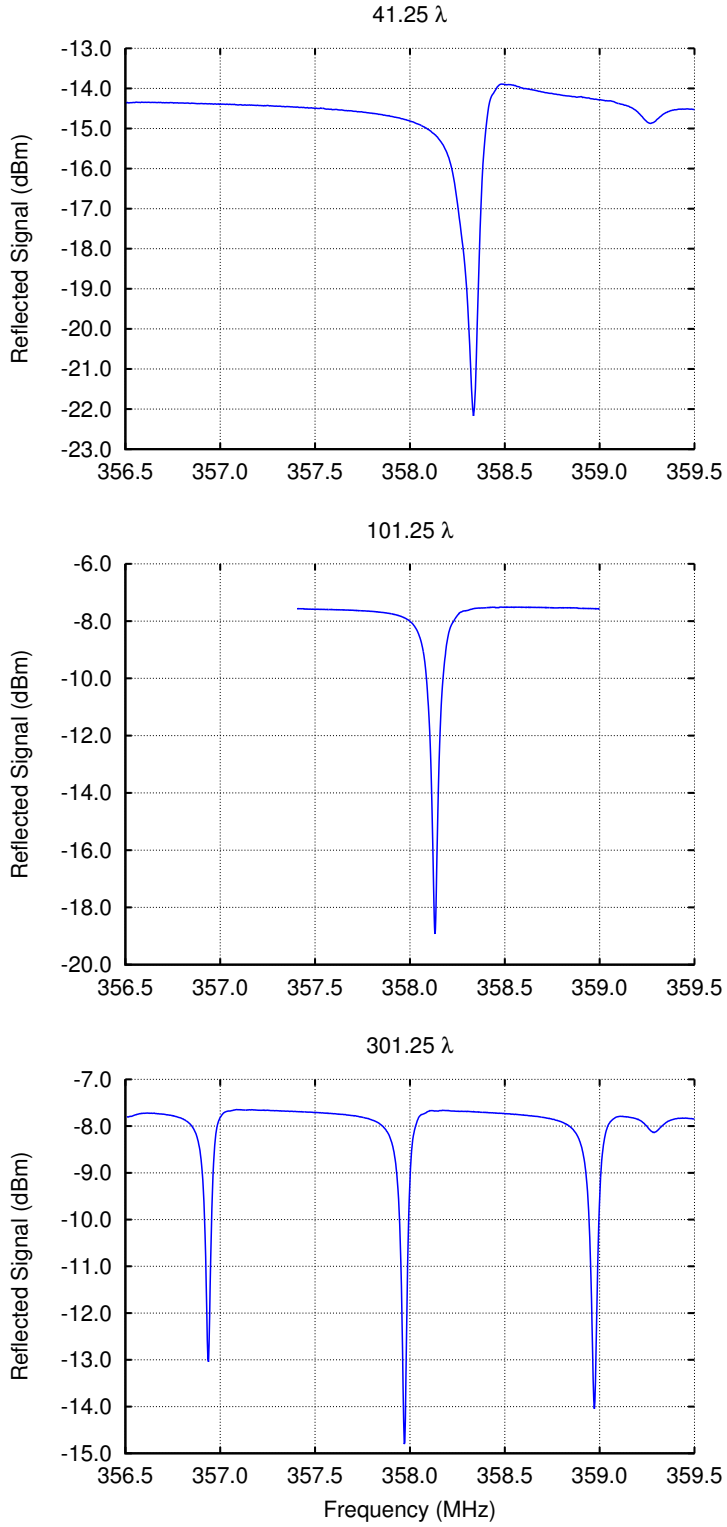

Figure 28.: *Comparison between different cavity dimensions for resonators on GaAs with emitter IDT of 40 pairs and mirrors composed by $n_g = 500$ strips .Input signal 10dBm.*

In figure 27 two resonators with the same mirrors but with 20 and 40 IDT pairs respectively are compared. As we can see the bandwidth is almost the same, although the 40 pairs IDT collect more energy from the cavity ($\approx$ 3dB).

The devices of the last mask are displayed in table 4. Before designing this mask we know that the best results were obtained with the emitter composed by 40 pairs, and with mirror composed by 500 strips. Moreover, the longer the IDT fingers the larger is the energy collected, therefore we design devices with $l = 100\lambda$. Finally in order to maximize the reflectivity of each electrode in the gratings, we deposited 100nm of aluminum (see section 1.5.1 and figure 7 in particular).

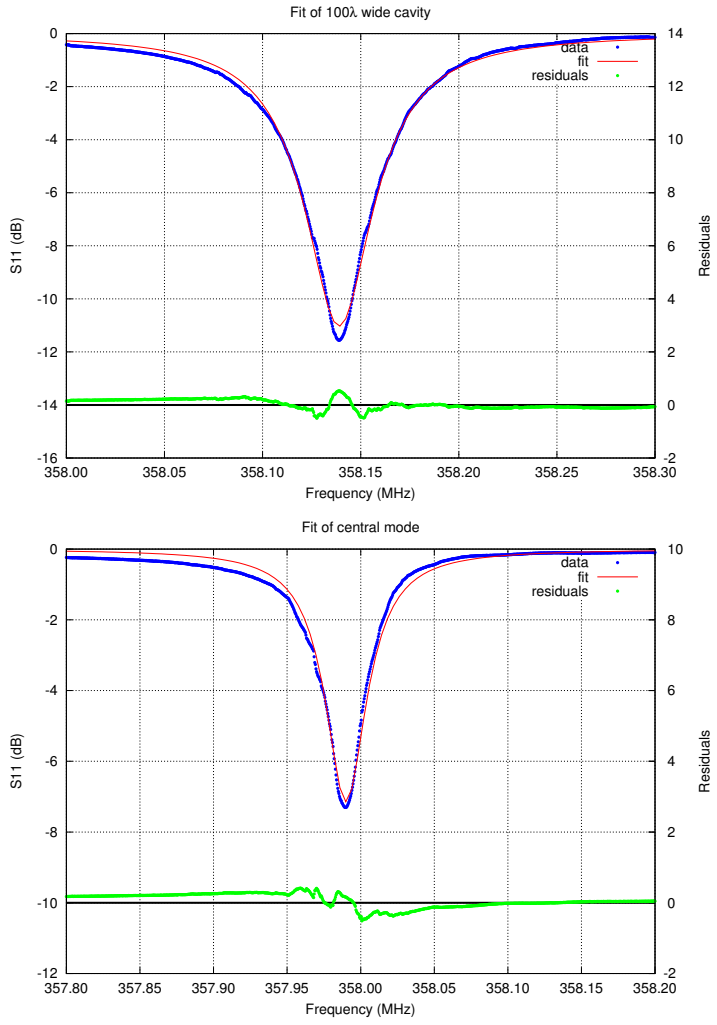

Figure 29.: *Fit of resonators on GaAs with emitter IDT of 40 pairs and mirrors composed by $n_g = 500$ strips, with cavity of 100λ and 300λ.*

The spectrum of the devices is presented in figure 28. The amplitude of the signal is very large, and the bandwidth is narrower than the same devices fabricated before. The fit of the real part of the reflection coefficient S_{11} (see the electrical equivalent model in appendix A) gives for the resonator with the 101.25λ wide cavity

$$Q_i = (2.75 \pm 0.01) \cdot 10^4 \qquad \text{and} \qquad Q_e = (0.79 \pm 0.01) \cdot 10^4, \quad (3.2)$$

and for the central deep of the resonator with 301.25λ cavity

$$Q_i = (5.00 \pm 0.03) \cdot 10^4 \qquad \text{and} \qquad Q_e = (1.02 \pm 0.01) \cdot 10^4. \quad (3.3)$$

3.2.3 *Impulse Measurements*

When the IDT emitter of a resonator is excited with a modulated pulse, the two mechanical wave packets (one in each directions) are reflected if their frequency f is within the mirror **stop band** Δf. Figure 30 presents a study in the time domain of the last device showed in figure 28.

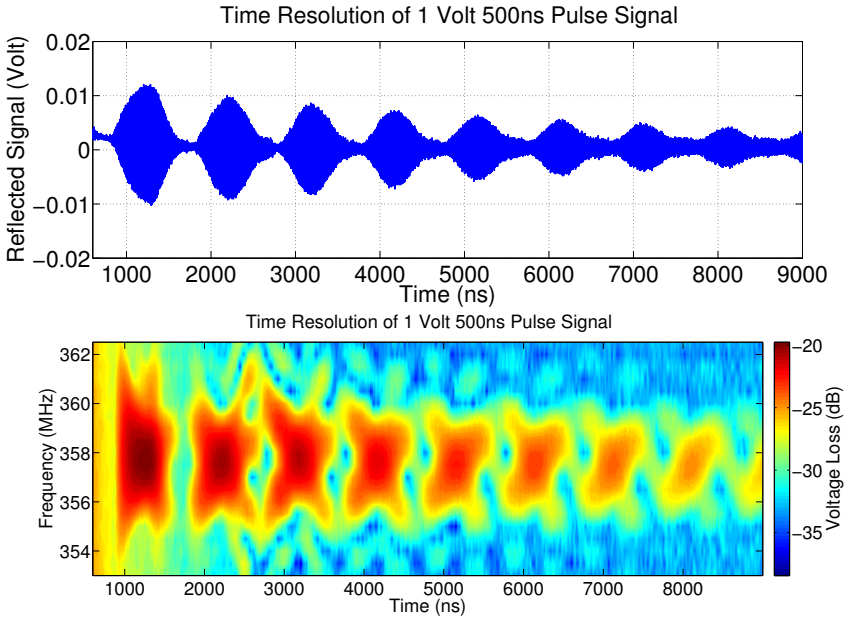

Figure 30.: *Pulse of 500ns on a resonator with emitter of 40 pairs, and mirror distant* 301.25λ.

A 500ns microwave burst at frequency f and amplitude 1 V is applied to the IDT, and the signal reflected from the same IDT is read out through the directional coupler by means of the oscilloscope. The envelope of the signal is converted in dB and then smoothed. The process is repeated for frequencies ranging

between $345 - 355$ MHz and then all data are merged (see figure 30).

This resonator has an IDT composed by 40 pairs, the mirror grating of 500 lines, and a cavity of 301.25 λ, and as we have seen it presents three resonances (see figure 28). Because the two pulse lengths are smaller than the cavity, they do not interfere, and the whole stop band of the mirror is visible in this figure 30.

It is important to notice that each time the pulses pass through the IDT, their amplitude decreases. This is due to three factors: the **reflection coefficient of mirror** is not exactly 1, therefore a tiny amount of energy is transmitted, the **mechanical and electrical losses** (see section 3.1.2) due to the strain viscosity, usually neglected, becomes important when the pulses travel for long time, and finally part of the energy is consumed during the **process of measurement**.

If the last energy loss is much smaller then the fist two, the ratio between the time of extinction of the pulses and the time of one oscillation can give an estimation of the **Q factor**: considering that $f \approx 357$MHz, and that the pulses looses all their energy in $\Delta t \approx 20\mu s$

$$Q \approx f \cdot \Delta t = 7000. \tag{3.4}$$

In this way we underestimate the quality factor, but its order of magnitude is compatible with the one measured in (3.3).

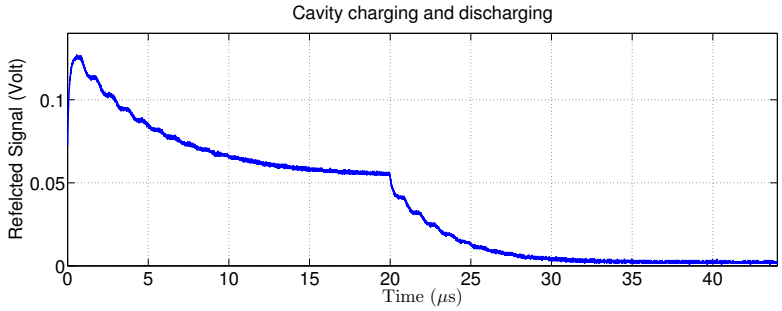

Figure 31.: *Pulse of* 20µs *that charges the cavity of a resonator with emitter of 40 pairs, and mirror distant* 301.25λ.

Instead of numerical estimate the envelope of the signal,it is possible to use a **diode** with a discharge time short enough to follow the signal amplitude variation, but large enough to maintain its charge during the periodic oscillations. Figure 31 shows the reflected signal pulse of a 20µs microwave burst of 1 V amplitude, applied to the IDT of the same device. From the exponential decreasing of the reflected signal is clear how the cavity suddenly starts to charge. After a period of about 20µs the cavity is fully excited, in fact the amplitude of transmitted signal reaches a plateau.

At this point the external source is suppressed, and the cavity starts to discharge. As for the charging process, this process takes about 20µs.

By changing the microwave frequencies it is possible to realize the plot displayed in figure 32.

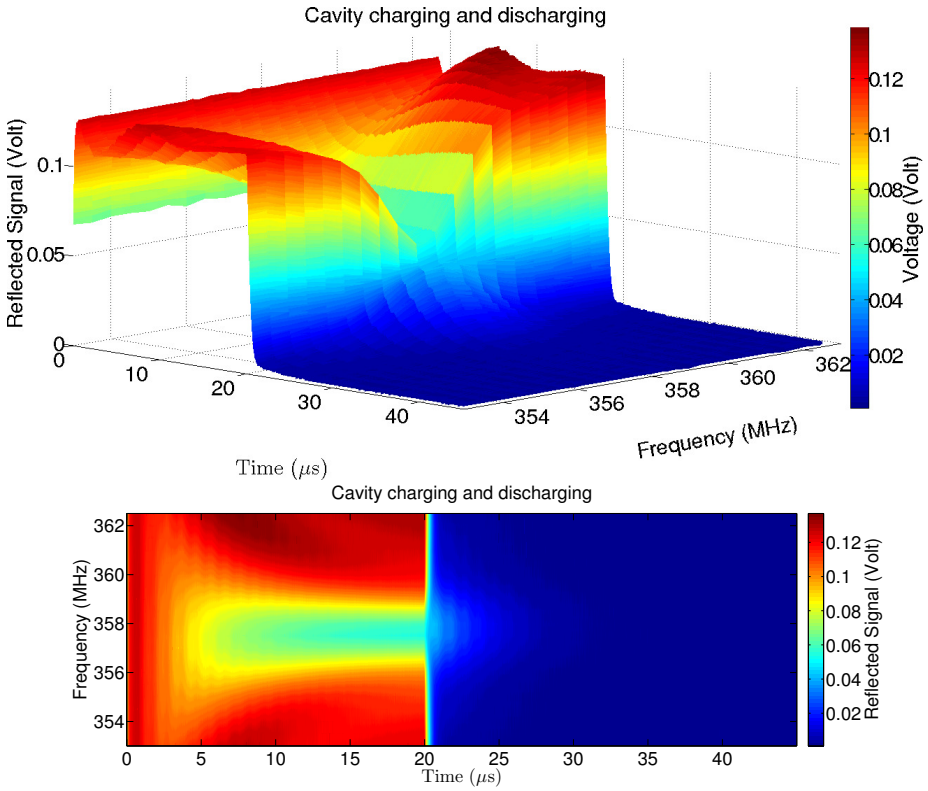

Figure 32.: *Stop Band of 500 lines mirror, underlines by a pulse of* 20µs *that charges the cavity of a resonator with emitter of 40 pairs, and mirror distant* 301.25λ.

The mirror stop band is clearly visible, and is about $\Delta f \approx 3$MHz. Therefore it is possible to estimate the **modulus of the reflection coefficient** for a single line on GaAs at room temperature:

$$|r| \approx \pi \frac{\Delta f}{2 f_0} \approx 0.013. \tag{3.5}$$

With this value it is possible to design multi-modes cavities and to calculate the number of their modes (see section 1.5.2).

3.2.4 *Resonator and Light Excitement*

Our devices are fabricated prevalently on GaAs that is a semiconductor, with a **direct energy gap** of 1.4eV. This means that light with a wavelength of 890nm can excite an electron from valence to

conduction band. When a SAW travel on the surface illuminated by a source with this wavelength, the coupled electric field acts on the free electrons promoted in the upper band. Because they are free, they start to move in the semiconductor dissipating energy.

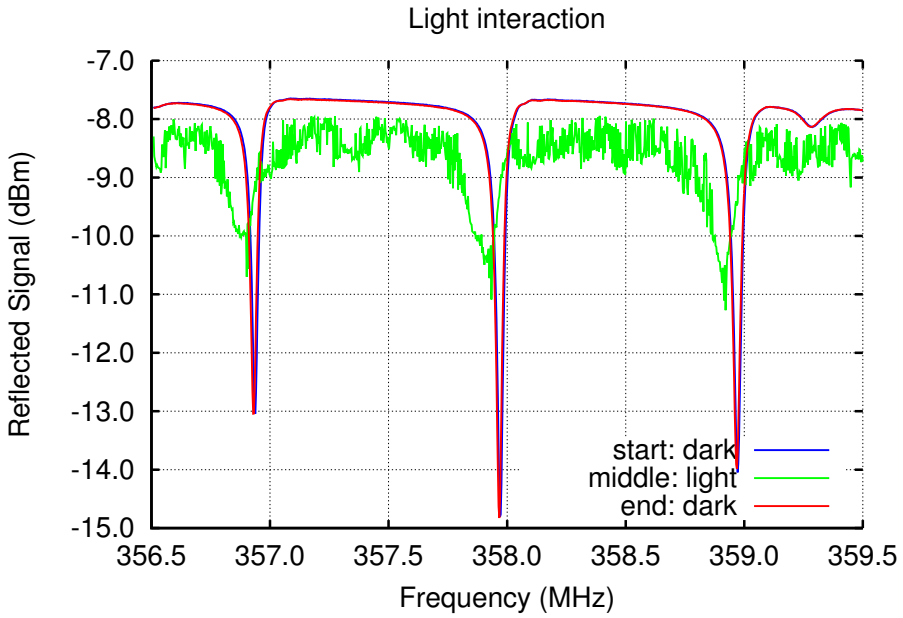

Figure 33.: *Interaction of light and a resonator with emitter of 40 pairs, and mirror distant* 301.25λ.

Figure 33 shows the different spectrum of a resonator with 3 modes, before the interaction with light, measured in a **black box**, then illuminated with a wide spectrum light, and again in the black box. As we can see, the Q factor of resonator drops significantly when the light is on. This is because the electrons dissipate more energy in each cycle than before, when they were confined in the valence band. For the same reason the signal goes from very smooth to very rough and irregular.

4

FINITE ELEMENT METHOD SIMULATIONS

4.1 FINITE ELEMENT METHOD

The equations of motion with free surface boundary condition can be solved analytically only with perturbative methods (see [7]). Their solutions describe the motion of a Rayleigh wave in a piezoelectric material.

In order to study the dynamics of the generation of this wave, we need to consider the piezoelectric substrate with a filter on it. The presence of an IDT and of an oscillating potential applied to it, imposes the setting of very structured boundary conditions. For this reason a numerical study of the system has been carried out with the finite element method.

Following [6], the **finite element method** consists in the application of the classical variational method to the union of small domains, called elements and connected to other elements by a finite number of nodes. This method most important features are:

- **Discretization**: the whole system is decomposed in the sum of pieces of finite dimension, the elements; their shape varies in function of the geometry and the number of spatial dimensions

- **Interpolation**: the solution is calculated only in the nodes, but can be reconstruct in the whole domain using different interpolation functions (called shape functions).

The displacement and the electrical potential in the i-th node of a single element are respectively $\mathbf{u}_i$ and ϕ_i. The corresponding continuous fields can be expressed using the shape function $\mathbf{N}_{\mathbf{u}i}(\mathbf{x})$ and $N_{\phi i}(\mathbf{x})$:

$$\mathbf{u}(\mathbf{x}) = \mathbf{N}_{\mathbf{u}i}(\mathbf{x}) \cdot \mathbf{u}_i \quad \text{and} \quad \phi(\mathbf{x}) = N_{\phi i}(\mathbf{x})\phi_i. \tag{4.1}$$

These functions, usually polynomial, have different number of coefficients depending on the problem equations. The values of the coefficients are fixed imposing that these functions assume the exact value at each node:

$$\mathbf{N}_i(x_i, y_i) = \mathbf{I}, \tag{4.2}$$

but since the value in the nodes is unknown, the nodes values become the new unknowns of the problem.

Using the Voigt notation, the strain and the electric field are obtained just with the substitution in the definition:

$$s(\mathbf{x}) = \mathcal{D}\mathbf{u}(\mathbf{x}) = \mathcal{D}\mathbf{N}_{\mathbf{u}i}(\mathbf{x}) \cdot \mathbf{u}_i := \mathbf{B}_{\mathbf{u}i}(\mathbf{x})\mathbf{u}_i, \tag{4.3}$$

and

$$\phi(\mathbf{x}) = -\nabla N_{\phi i}(\mathbf{x})\phi_i := -B_{\phi i}(\mathbf{x})\phi_i, \tag{4.4}$$

where the functions B_i are the derivative of shape functions, and $\mathcal{D}$ is the differential operator

$$\mathcal{D} = \begin{pmatrix} \partial_x & 0 & 0 \\ 0 & \partial_y & 0 \\ 0 & 0 & \partial_z \\ 0 & \partial_z & \partial_y \\ \partial_z & 0 & \partial_x \\ \partial_y & \partial_x & 0 \end{pmatrix} \tag{4.5}$$

In order to find out the equation for the unknowns $\mathbf{u}_i$ and ϕ_i we can use the **Hamilton principle**

$$\delta \int_{t_1}^{t_2} (L + W)\,dt = 0. \tag{4.6}$$

where L is the system Lagrangian and W is the work of external mechanical and electrical forces. The former can be derived as a Legiandre transformation of the Hamiltonian expressed in (1.91):

$$L = \int_V \left[\frac{1}{2}\rho\dot{\mathbf{u}}^2 - \left(\frac{1}{2}\mathbf{s}^t c\mathbf{s} - \mathbf{E}^t e\mathbf{s} - \frac{1}{2}\mathbf{E}^t \epsilon \mathbf{E}\right)\right] dV. \tag{4.7}$$

The ladder is the sum of the works produced mechanically by volume forces $\mathbf{F}_V$, surface forces $\mathbf{F}_\Omega$ and point forces $\mathbf{F}_P$, ad the works produced electrically by the total charge Q and the surface charge q. If the displacement is infinitesimal ($\delta\mathbf{u}$):

$$\begin{aligned} \delta W = &\int_V (\delta\mathbf{u} \cdot \mathbf{F}_V)\, dV + \int_{\Omega_1} (\delta\mathbf{u} \cdot \mathbf{F}_\Omega)\, d\Omega + \delta\mathbf{u} \cdot \mathbf{F}_P + \\ &- \int_{\Omega_2} (\delta\phi q)\, d\Omega - \delta\phi Q. \end{aligned} \tag{4.8}$$

The Hamilton principle is then written

$$\begin{aligned} 0 = &- \int_V \left[\rho\delta\mathbf{u}^t\ddot{\mathbf{u}} - \delta\mathbf{s}^t c\mathbf{s} + \delta\mathbf{s}^t e\mathbf{E} + \delta\mathbf{E}^t e\mathbf{s} + \delta\mathbf{E}^t \epsilon\mathbf{E} + \delta\mathbf{u}^t\mathbf{F}_V\right] dV + \\ &+ \int_{\Omega_1} \left(\delta\mathbf{u}^t\mathbf{F}_\Omega\right) d\Omega - \int_{\Omega_2} (\delta\phi q)\, d\Omega + \\ &+ \delta\mathbf{u}^t\mathbf{F}_P - \delta\phi Q \end{aligned} \tag{4.9}$$

Using the discretization (4.3) and (4.4):

$$\begin{aligned}
0 =& -\delta\mathbf{u}_i^t \int_V \left(\rho \mathbf{N}_{\mathbf{u}j}^t \mathbf{N}_{\mathbf{u}j}\right) dV \ddot{\mathbf{u}}_i - \delta\mathbf{u}_i^t \int_V \left(\rho \mathbf{B}_{\mathbf{u}j}^t c \mathbf{B}_{\mathbf{u}j}\right) dV \mathbf{u}_i \\
&- \delta\mathbf{u}_i^t \int_V \left(\rho \mathbf{B}_{\mathbf{u}j}^t e B_{\phi j}\right) dV \phi_i - \delta\phi_i^t \int_V \left(\rho \mathbf{B}_{\phi j}^t e \mathbf{B}_{\mathbf{u}j}\right) dV \mathbf{u}_i \\
&+ \delta\phi_i^t \int_V \left(\rho \mathbf{B}_{\phi j}^t \epsilon \mathbf{B}_{\phi j}\right) dV \phi_i + \delta\mathbf{u}_i^t \int_V \left(\rho \mathbf{N}_{\mathbf{u}i}^t \mathbf{F}_V\right) dV \\
&+ \delta\mathbf{u}_i^t \int_{\Omega_1} \left(\rho \mathbf{N}_{\mathbf{u}i}^t \mathbf{F}_\Omega\right) d\Omega - \delta\phi_i^t \int_{\Omega_2} \left(N_{\phi i}^t q\right) d\Omega \\
&+ \delta\mathbf{u}_i^t \mathbf{N}_{\mathbf{u}i}^t \mathbf{F}_P - \delta\phi_i^t N_{\phi i}^t Q
\end{aligned} \tag{4.10}$$

If we define the **element mass**

$$M = \int_V \left(\rho \mathbf{N}_{\mathbf{u}j}^t \mathbf{N}_{\mathbf{u}j}\right) dV, \tag{4.11}$$

the **element stiffness**

$$K_{\mathbf{uu}} = \int_V \left(\rho \mathbf{B}_{\mathbf{u}j}^t c \mathbf{B}_{\mathbf{u}j}\right) dV, \tag{4.12}$$

the **piezoelectric coupling**

$$K_{\mathbf{u}\phi} = \int_V \left(\rho \mathbf{B}_{\mathbf{u}j}^t e B_{\phi j}\right) dV, \tag{4.13}$$

the **element capacitance**

$$K_{\phi\phi} = -\int_V \left(\rho \mathbf{B}_{\phi j}^t \epsilon \mathbf{B}_{\phi j}\right) dV, \tag{4.14}$$

and the external **mechanical** and **electrical** forces

$$\mathbf{f}_i = \int_V \left(\rho \mathbf{N}_{\mathbf{u}i}^t \mathbf{F}_V\right) dV + \int_{\Omega_1} \left(\rho \mathbf{N}_{\mathbf{u}i}^t \mathbf{F}_\Omega\right) d\Omega + \mathbf{N}_{\mathbf{u}i}^t \mathbf{F}_P \tag{4.15}$$

$$g_i = -\int_{\Omega_2} \left(N_{\phi i}^t q\right) d\Omega - N_{\phi i}^t Q, \tag{4.16}$$

the finite element method equations become

$$\begin{aligned}
M\ddot{\mathbf{u}}_i + K_{\mathbf{uu}}\mathbf{u}_i + K_{\mathbf{u}\phi}\phi_i &= \mathbf{f}_i \\
K_{\phi\mathbf{u}}\mathbf{u}_i + K_{\phi\phi}\phi_i &= g_i
\end{aligned} \tag{4.17}$$

4.2 COMSOL SIMULATION

4.2.1 *Geometry and Boundary Conditions*

The system chosen for the simulation is a filter located on a lithium niobate substrate. The dimension of a single finger is

$w = 2.8\mu m$ and the number of IDT pairs is $n_p = 10$ for both emitter and receiver IDT. The receiver IDT is placed at 10λ from the emitter. The total dimension of the substrate is $34\lambda = 380\mu m$ long and $2\lambda = 22\mu m$ high.

The IDT are represented only as electrical boundary conditions: the electrode are therefore perfect conductor without impedance. This means that the mechanical component of the single strip reflection coefficient is neglected (see equation (1.112)): this does not affect the filter simulations, but it can be very important for the resonators simulation.

The mechanical boundary conditions are:

- **Free surface**: $\sigma_{i2} = 0$ for the upper surface $y = 22\mu m$;
- **Damped surface**: $\sigma_{i2} = d\partial_t u_i$ for lower surface $y = 0$, and $\sigma_{i1} = -d\partial_t u_i$ for lateral surface $x = 0\mu m$ and $x = 380\mu m$.

And the electrical one

- **Zero charge**: $\mathbf{D} \cdot \hat{\mathbf{n}} = 0$ for all the surface except the electrodes;
- **Charge conservation**: $\nabla \cdot \mathbf{D} = \rho$ for the volume.

4.2.2 *Mesh and Courant Condition*

The mesh of SAW simulation is a very critical problem because of both large spatial domain and small features of device. The former limits the element dimension because of the memory and the time needed to obtain a solution, the latter fixes the smallest dimension of an element.

Moreover the presence of traveling waves imposes that the algorithm of numerical integration must update the solution faster than the deformation propagation in the material. Defining the **numerical velocity**

$$v_n = \frac{\Delta x}{\Delta t} \tag{4.18}$$

where Δx is the smallest element dimension and Δt the integration time step, we have to impose the **Courant condition**:

$$C := \frac{v}{v_n} < 1; \tag{4.19}$$

where C is the Courant number. Therefore there are two possibilities: to make larger elements, or to choose a smaller time step. As already said, in our system the maximum dimension of an

element is fixed by the finger dimension, therefore using $C = 0.2$ and $\Delta x = \frac{w}{2}$ the time step results to be

$$\Delta t = \frac{w}{10v} = \frac{1}{40f_0} \tag{4.20}$$

4.2.3 *Simulation Results*

An oscillating potential of 10 V is applied to the emitter: the generated SAWs travel until they reach the second IDT.

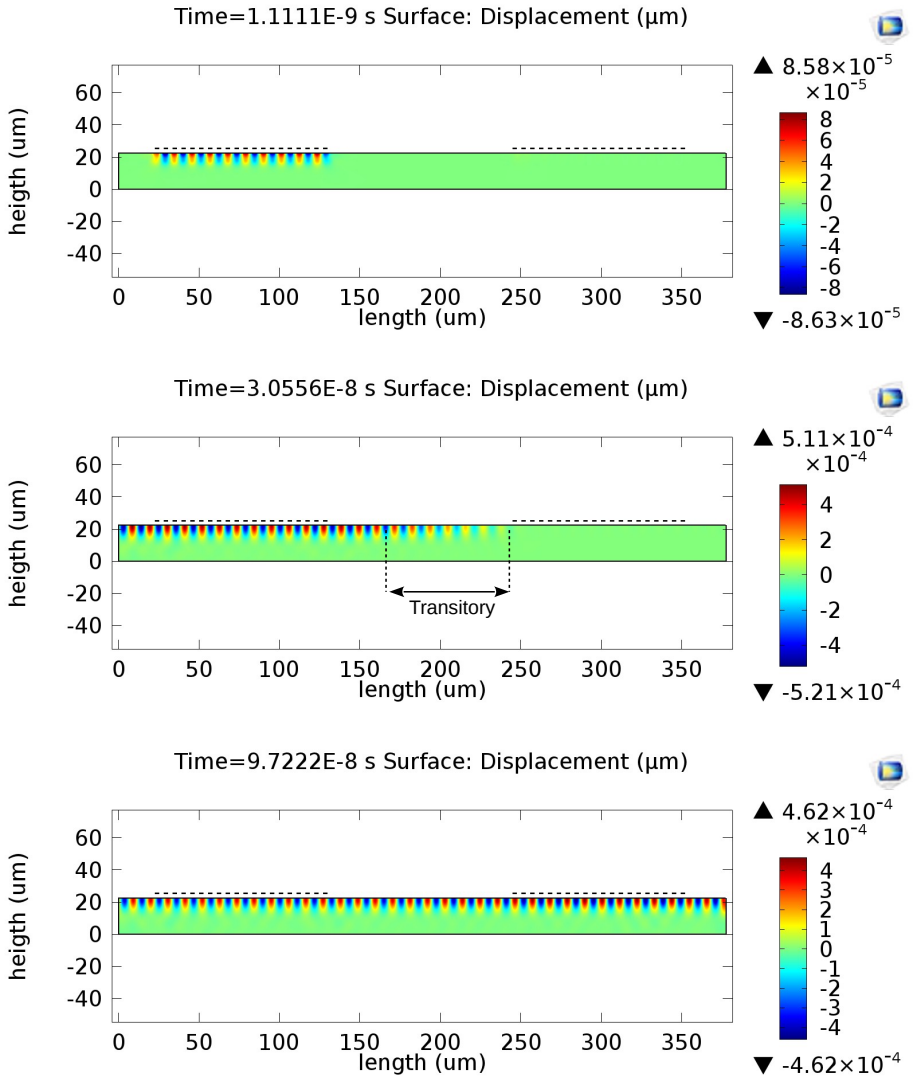

Figure 34.: *Time evolution of SAWs launched by 10 pairs IDT at the resonance frequency of 360 MHz.*

The evolution of this system is shown in figure 34:

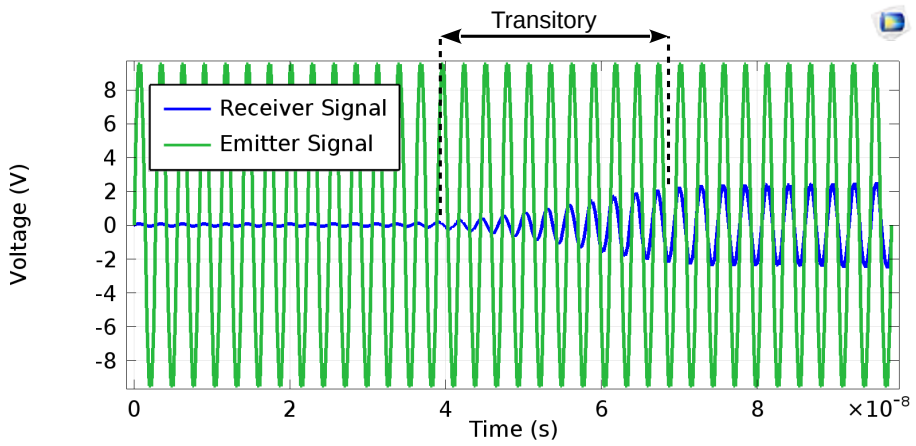

Figure 35.: *Comparison between the emitted and the received signal at resonance frequency of 360 MHz.*

- the first plot shows the generation of the SAW after the first oscillation of the potential; the maximum displacement of $8.6 \cdot 10^{-5}\mu m$, displayed in the side color-bar is in accordance with equation (1.23);

- the second plot presents the propagation of the SAWs toward the receiver IDT; in the wave front, underlined in the picture, is evidently present a transitory: the amplitude of displacement goes from the initial value of $8.6 \cdot 10^{-5}\mu m$ to the maximum value of $5.1 \cdot 10^{-5}\mu m$ almost an order of magnitude larger;

- in the last plot it is displayed the stationary regime reached after fifty potential oscillations; it is clearly visible that the SAWs amplitudes are constant through the whole substrate.

These steps in the temporal evolution are found again in the plot of the electric signal on the receiver IDT in figure 35):

- since the distance between the two IDTs is 120 μm the initial signal from 0 to 40 ns is zero;

- when the wave front reaches the receiver IDT, a transitory is visible from 40 to 70 ns ; this temporal delay is the time in which the SAWs goes through the whole 10 IDT pairs of the emitter, i.e. the time in which the stationary state is reached;

- after 70 ns the signal is stationary at maximum value of 2V.

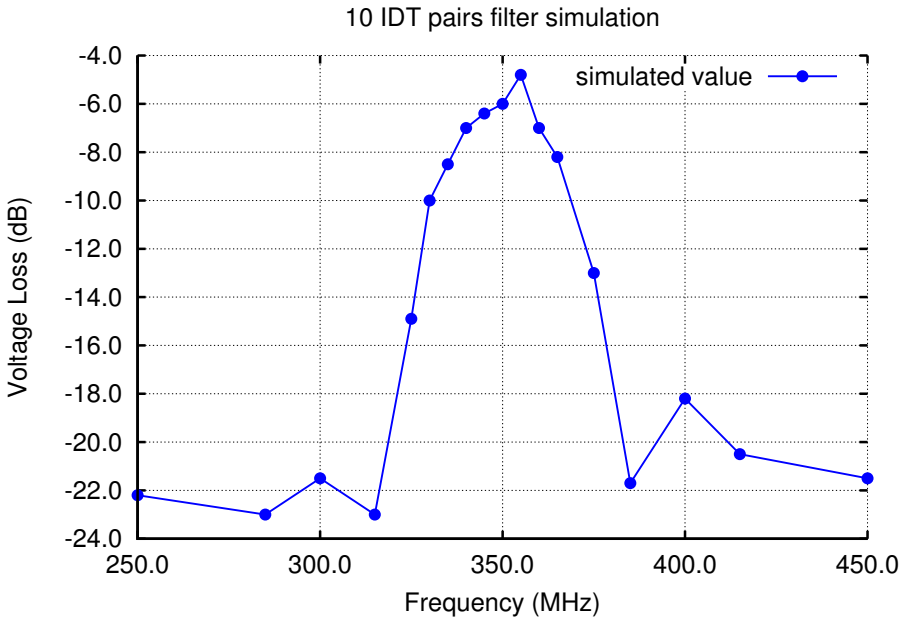

Figure 36.: *Simulated spectrum of filter with 10 IDT pairs (values in table 5).*

Frequency (MHz)	Receiver IDT Voltage (V)	voltage loss $\frac{V_{out}}{V_{in}}$ (dB)
250	0.06	-22.2
285	0.05	-23.0
300	0.07	-21.5
315	0.05	-23.0
325	0.4	-14.9
330	1.0	-10.0
335	1.4	-8.5
340	2.0	-7.0
345	2.3	-6.4
350	2.5	-6.0
355	3.0	-4.8
360	2.0	-7.0
365	1.5	-8.2
370	0.8	-11.0
375	0.5	-13.0
385	0.08	-21.7
400	0.15	-18.2
415	0.09	-20.5
450	0.07	-21.5

Table 5.: *Signal on receiver IDT at different frequencies, with 10 V signal on the emitter IDT.*

In order to calculate the frequency response of the filter, this simulation has been repeated for different frequencies and the results are presented in table 5. These values are plotted in figure 36.

As expected from 1.31 the bandwidth is about 60 MHz. The spectrum shape is similar to the expected one (see section 3.1.2). In order to have more frequency definition, a larger number of simulations is needed.

Anyway, these results show that this model and simulation permit to catch the main physics and device response properties of the SAW filter.

Thus, a tool is now available for the design and optimization of SAW devices and it can be also applied on different, innovative materials to extract their unknown electromechanical properties.

A

ELECTROTECHNIC

Each measurement in this works has been carried though an electric cable, and SAW devices are themselves electric components of the circuit. Therefore it is worth a brief introduction on how signal transfer works.

A.1 PORT NETWORK MODEL

A.1.1 *Scattering Matrix*

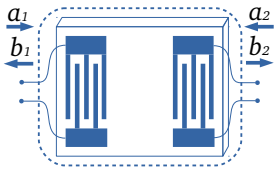

Two port model for SAW filters

At electric level a SAW filter is a box with an input and an output port: despite the physical phenomena that transfer the signal in the box, the measure concerns only the amplitude and phase of signals. A signal is an oscillating difference of potential between two terminals (therefore a 2 port network has 4 terminals) and it can be expressed by a complex number where its module is the voltage amplitude and the complex phase is the voltage phase.

Suppose that a signal a_1 enters in the box from port 1, ad another signal a_2 comes in the box from port 2. A **complex** fraction S_{21} of the signal a_1 pass through the network and a complex fraction S_{22} of signal a_2 is reflected by the network. So that a signal $b_2 = S_{21}a_1 + S_{22}a_2$ is present at the port 2. In the same way a signal $b_1 = S_{12}a_2 + S_{11}a_1$ can be detected at port 2. Writing this relations in matrix form we obtain the so called **scattering parameters** (S-parameters):

$$\begin{pmatrix} b_1 \\ b_2 \end{pmatrix} = \begin{pmatrix} S_{11} & S_{12} \\ S_{21} & S_{22} \end{pmatrix} \begin{pmatrix} a_1 \\ a_2 \end{pmatrix}. \tag{A.1}$$

If the network has no losses (or gains), the energy of incident signal is equal to the leaving one; this means that

$$|a_1|^2 + |a_2|^2 = |b_1|^2 + |b_2|^2. \tag{A.2}$$

If $a_2 = 0$ then

$$|S_{11}|^2 + |S_{12}|^2 = 1, \tag{A.3}$$

and if $a_1 = 0$

$$|S_{22}|^2 + |S_{21}|^2 = 1. \tag{A.4}$$

Using these last two relations, when $a_1 \neq 0$ and $a_2 \neq 0$

$$(S_{21}S_{22}^* + S_{11}S_{12}^*)\, a_1 a_2^* + (S_{12}S_{11}^* + S_{11}S_{21}^*)\, a_2 a_1^* = 0. \tag{A.5}$$

Setting $a_1 a_2^*$ to be real or imaginary, and subtracting the two results, we have:

$$S_{11}S_{12}^* + S_{22}^*S_{12} = 0. \tag{A.6}$$

SAW filters designed in this thesis present a **symmetry** for port 1 and 2, this means that the matrix is symmetric itself $S_{12} = S_{21}$, therefore the reflection coefficient S_{11} and S_{22} are pure imaginary number.

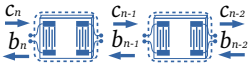

Cascade configuration.

Consider a **cascade configuration** of N elements: it is useful to have a scattering matrix for the signals at the extremes of the network, b_N and c_0 in function of c_N and b_0. Therefore considering the scattering matrix for the $n-$th element, with the configuration shown in the picture we have

$$\begin{pmatrix} b_n \\ c_{n-1} \end{pmatrix} = \begin{pmatrix} s_{11} & s_{12} \\ s_{21} & s_{22} \end{pmatrix} \begin{pmatrix} c_n \\ b_{n-1} \end{pmatrix}. \tag{A.7}$$

Solving this system for c_n and b_n gives

$$\begin{pmatrix} c_n \\ b_n \end{pmatrix} = \begin{pmatrix} \frac{1}{s_{21}} & -\frac{s_{22}}{s_{21}} \\ \frac{s_{11}}{s_{21}} & s_{12} - \frac{s_{11}s_{22}}{s_{21}} \end{pmatrix} \begin{pmatrix} c_{n-1} \\ b_{n-1} \end{pmatrix}. \tag{A.8}$$

If every element does not present energy loss and it is symmetric $s_{11} = s_{22} = t$ and $s_{12} = s_{21} = r$, therefore

$$\begin{pmatrix} c_N \\ b_N \end{pmatrix} = \begin{pmatrix} \frac{1}{t} & -\frac{r}{t} \\ \frac{r}{t} & \frac{1}{t} \end{pmatrix}^N \begin{pmatrix} c_0 \\ b_0 \end{pmatrix}. \tag{A.9}$$

If $N \gg 1$ the solution can be approximated with **Bloch modes** $c_n = c_{n-1}e^{-i\theta}$ and $b_n = b_{n-1}e^{-i\theta}$; solving the system:

$$\begin{cases} c_n = \frac{1}{t}c_{n-1} + \frac{r}{t}b_{n-1} = e^{-i\theta}c_{n-1} \\ b_n = -\frac{r}{t}c_{n-1} + \frac{1}{t}b_{n-1} = e^{-i\theta}b_{n-1} \end{cases} \tag{A.10}$$

we obtain

$$\begin{cases} \frac{1}{t} = \frac{1}{2}\left(e^{i\theta} + e^{-i\theta}\right) = \cos(\theta) \\ \frac{r}{t} = \frac{1}{2i}\left(e^{i\theta} - e^{-i\theta}\right) = \sin(\theta) \end{cases}. \tag{A.11}$$

Diagonalizing the matrix we obtain the eigenvalue $e^{\pm i\theta}$ with eigenvector $(1, \pm i)$. Therefore introducing the matrix of change of basis, the new signals are:

$$\begin{pmatrix} u_n \\ v_n \end{pmatrix} = \begin{pmatrix} 1 & 1 \\ i & -i \end{pmatrix}^{-1} \begin{pmatrix} c_n \\ b_n \end{pmatrix} = \begin{pmatrix} \frac{1}{2}(c_n - ib_n) \\ \frac{1}{2}(c_n + ib_n) \end{pmatrix}, \tag{A.12}$$

and the equation (A.9) becomes

$$\begin{pmatrix} u_N \\ v_N \end{pmatrix} = \begin{pmatrix} e^{iN\theta} & 0 \\ 0 & e^{-iN\theta} \end{pmatrix} \begin{pmatrix} u_0 \\ v_0 \end{pmatrix}. \tag{A.13}$$

Coming back to the original basis we have

$$\begin{pmatrix} c_N \\ b_N \end{pmatrix} = \begin{pmatrix} \frac{1}{2}\left(e^{iN\theta} + e^{-iN\theta}\right) & -\frac{1}{2i}\left(e^{iN\theta} - e^{-iN\theta}\right) \\ -\frac{1}{2i}\left(e^{iN\theta} - e^{-iN\theta}\right) & \frac{1}{2}\left(e^{iN\theta} + e^{-iN\theta}\right) \end{pmatrix} \begin{pmatrix} c_0 \\ b_0 \end{pmatrix}. \tag{A.14}$$

Finally rewriting it in terms of global scattering matrix

$$\begin{pmatrix} c_0 \\ b_N \end{pmatrix} = \begin{pmatrix} S_{11} & S_{12} \\ S_{21} & S_{22} \end{pmatrix} \begin{pmatrix} b_0 \\ c_N \end{pmatrix}, \tag{A.15}$$

we have

$$\begin{aligned} S_{11} = S_{22} &= \frac{1}{\cos(N\theta)} \\ S_{12} = S_{21} &= -\tan(N\theta) \end{aligned}. \tag{A.16}$$

A.1.2 *Instruments Measurement*

When devices are measured, the signal is applied only at one port, i.e. $a_2 = 0$. Using the previous equations we can define the **transmitted signal** $b_2 = S_{21}a_1$ and in the same way the **reflected signal** is $b_1 = S_{11}a_1$. With these conditions it is possible to consider the S-parameters as ratios:

$$S_{11} = \frac{b_1}{a_1} = \frac{\text{reflected signal}}{\text{input signal}}, \qquad S_{21} = \frac{b_2}{a_1} = \frac{\text{transmitted signal}}{\text{input signal}}. \tag{A.17}$$

We are supposing that the S-parameters are just complex numbers, i.e. they does not depend on the signal i.e the network is **linear**. This is not always true, but for the power used in our measurements the linearity holds. The IDT produces a deformation that travels on the surface: if the electric field is not too high this deformation is linear with the field. Figure 37 shows the response of the filter with different signal powers: unless the lower line, which is at at instrument noise level (-70 dBm), the data are all shifted by 10 dBm. In this hypothesis there is no need to specify the amplitude of incoming signal, because just the coefficients S_{11} and S_{21} specify the network response at any possible signal. Moreover because the variation of signals in SAW devices are of some order of magnitude, it is useful to express these coefficients in dB (remembering that they are ratios).

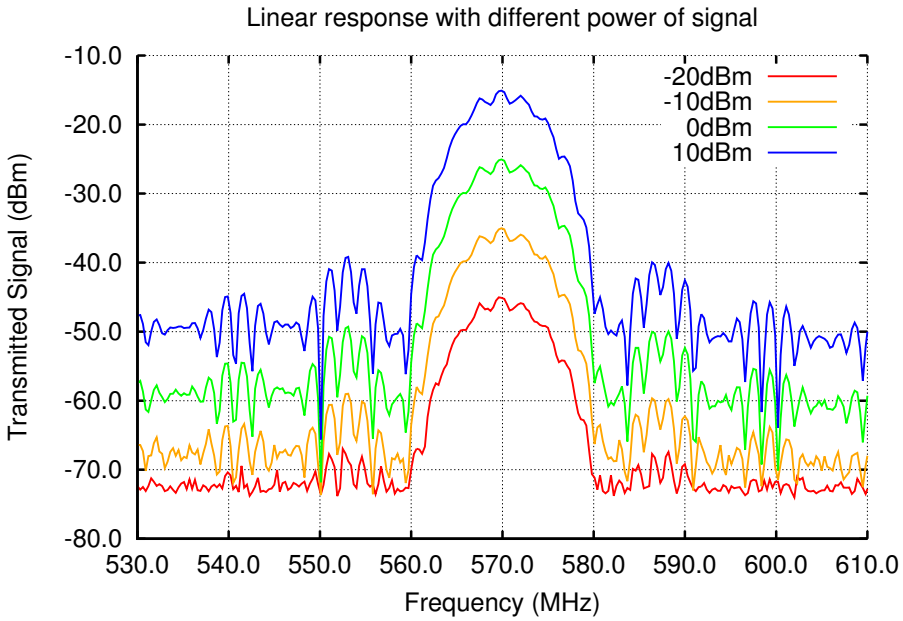

Figure 37.: *SAW filter with IDT of 40 pairs on 2 µm of GaN on Sapphire, exited with signals of different power.*

The signal generator produces a signal a_1, expressed in **dBm**, that is a measure of power supposing that there is a load R of **50Ω**. The power of a periodic signal is

$$P = \frac{V_{rms}^2}{R}, \tag{A.18}$$

$x dBm = 10^{\frac{x}{10}} mW$
10 dBm=10 mW
0 dBm=1 mW
-10 dBm=0.1 mW
-20 dBm=0.01 mW

where V_{rms} is the **root mean square** voltage, and for sinusoidal signal is

$$V_{rms} = \sqrt{\frac{1}{T}\int_0^T (V_p \sin(\omega t))^2 dt} = \frac{V_p}{\sqrt{2}}, \tag{A.19}$$

Where V_p is the voltage peak. The power of these signals is

$$P = \frac{V_p^2}{2R}. \tag{A.20}$$

With 50Ω load
10 dBm≈1000 mV
0 dBm≈300 mV
-10 dBm≈100 mV
-20 dBm≈30 mV

As a consequence, the conversion between dBm and mV with 50Ω load is

$$x(V) = \sqrt{\frac{10^{\frac{x(dBm)}{10}}}{10}}. \tag{A.21}$$

A.1.3 *P Matrix*

The study of the elements of SAW devices, like gratings or cavities, needs a quantity that controls the potential and the current

through each element. Introducing and additional electrical ports, and considering the other two port for acoustic signals, the **P-matrix** is:

$$\begin{pmatrix} b_1 \\ b_2 \\ I \end{pmatrix} = \begin{pmatrix} P_{11} & P_{12} & P_{13} \\ P_{21} & P_{22} & P_{23} \\ P_{31} & P_{32} & P_{33} \end{pmatrix} \begin{pmatrix} a_1 \\ a_2 \\ V \end{pmatrix} \tag{A.22}$$

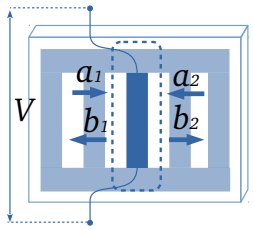

Three port model for elements of SAW devices.

If $V = 0$ with the same argument used for S-parameters, we have:

$$|P_{11}|^2 + |P_{12}|^2 = |P_{22}|^2 + |P_{21}|^2 = 1 \tag{A.23}$$

and

$$P_{11}P_{12}^* + P_{22}^*P_{12} = 0. \tag{A.24}$$

A.2 1 PORT RESONATORS

The Q factor defined in chapter 1 characterizes an unload resonator, and it is unaffected by any external electrical components. In the following we will call it Q_0.

The excitation and the measurement of a resonator signal inevitably reduce the total Q factor, because of energy losses in the feed line. Following [4] the total Q factor is

$$\frac{1}{Q} = \frac{1}{Q_0} + \frac{1}{Q_e}, \tag{A.25}$$

where Q_e, called **external quality factor**, is due to the electrical energy loss. Therefore it is not possible to measure directly the internal quality factor Q_0.

The equivalent circuit of 1 port resonator is presented in figure 38. The capacity C_0 is the static capacity due to the electric capacitor that each couple of fingers forms. The measurement of its value for our devices gives

$$C_0 \sim 1pF. \tag{A.26}$$

Actually this value sums up the static capacity of the PCB, of the bonding, and of course the resonator: therefore this value is an upper limit. R, C and L are the dynamic values of resistance, impedance and capacity: these values are different from zero only in the presence of a SAW. Since C is much larger than C_0 we will neglect the static capacity in the following.

The reflection coefficient for the equivalent circuit is given by

$$S_{11} = \frac{Z - Z_0}{Z + Z_0}, \tag{A.27}$$

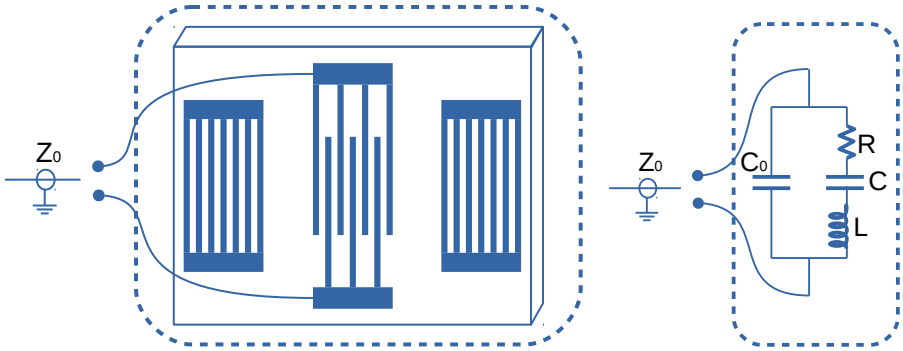

Figure 38.: *Equivalent circuit model for a SAW resonator.*

where Z_0 and Z are respectively the impedance of the feed line and the resonator:

$$Z(\omega) = R + i\omega L - i\frac{1}{\omega C} = R + i\omega L\left(1 - \frac{1}{\omega^2 LC}\right). \tag{A.28}$$

Defining the resonance $\omega_0 = \frac{1}{\sqrt{LC}}$ the internal Q-factor is

$$Q_0 = \omega_0 \frac{L}{R}. \tag{A.29}$$

Using the approximation around ω_0

$$(\omega^2 - \omega_0^2) = (\omega - \omega_0)(\omega + \omega_0) \approx 2\omega\Delta\omega, \tag{A.30}$$

the impedance becomes

$$Z(\omega) = R + i\omega L\left(\frac{\omega^2 - \omega_0^2}{\omega^2}\right) \approx R + i\frac{2RQ_0\Delta\omega}{\omega_0}. \tag{A.31}$$

Finally using the definition of external Q factor

$$Q_e = Q_0 = \omega_0 \frac{L}{Z_0}, \tag{A.32}$$

and the relation

$$\frac{\Delta\omega}{\omega_0} = \frac{\omega - \omega_0}{\omega_0} = \frac{f - f_0}{f_0} \tag{A.33}$$

the reflection coefficient for resonator is:

$$S_{11}(f) = \frac{\frac{Q_e - Q_0}{Q_e} + 2iQ_0\frac{f - f_0}{f}}{\frac{Q_e + Q_0}{Q_e} + 2iQ_0\frac{f - f_0}{f}}. \tag{A.34}$$

B

ERRORS TREATMENTS AND DATA ANALYSIS

B.1 ERRORS

The measurement of the signal from the Signal Generator through the shorted cables is shown in figure 39.

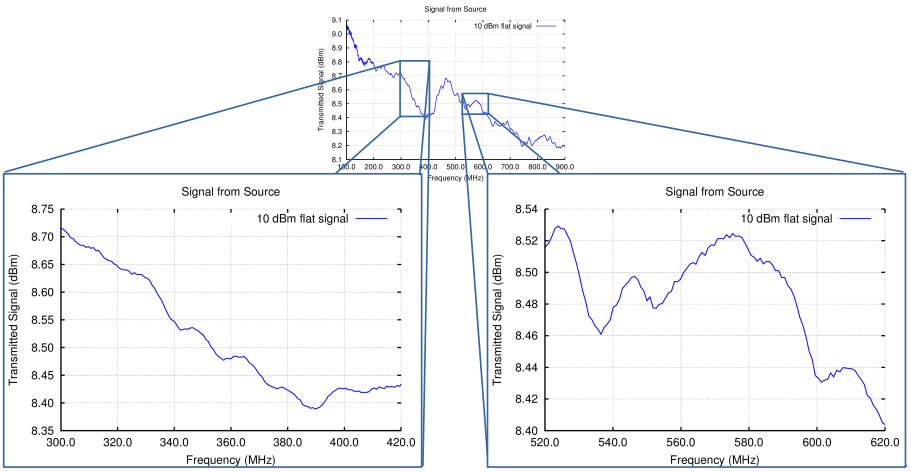

Figure 39.: *Shorted cables signal for 10 dBm input.*

The signal is not flat. In the frequency range from 300 MHz to 400MHz (the same of our measurements) there are random trends of 0.3dB amplitude. Since our measurements have almost always a larger signal, in a smaller range we decided to not subtract these trends.

B.2 DATA PLOTS

Data are plotted with the following gnuplot script:

```
set title "Plot Title"
set xlabel "Frequency (MHz)"
set ylabel "Transmitted Signal (dBm)"
set format x "%1.1s"  # %s=mantissa
set format y "%1.1s"  # 1.1=format
set grid    #grid on plot
set style line 1 lt 2 lc rgb "blue" lw 3  #line type 2,
    line color blue, line width 3
set xrange [530000000:610000000]
set border 3 lw 2 #border type 3 with line width 2
```

```
set terminal postscript eps color solid enhanced font 'Helvetica,20' #output file postscript, line solid, large font
set output 'plot_example.eps'
plot './data.dat' every ::6 w l ls 1 title "legend" #plot data, start from row 6, with line, line style 1, legend
```

gnuplot_plot.gnu

The plot of solution of Rayleigh waves for isotropic media is made with this matlab script:

```
[x,y] = meshgrid(0:0.25:10,0:-0.25:-2); %define the plot domain
u=cos(x).*(exp(0.8475*y)-0.5774*exp(0.3933*y)); % define the x component of the field
v=0.8475*cos(x).*exp(0.8475*y)-1.468*sin(x).*exp(0.3933*y); %define the y component of the field
hFig1=figure(1);     %define new plot window
set(hFig1, 'Position', [0 0 1500 750]); %set plot windows
quiver(x,y,u,v,'linewidth',2);  %plot vector field
set(gca,'fontsize',30); %set plot font size
xlabel('Relative position $\frac{x}{k_R}$','Interpreter','latex','FontSize', 30');
ylabel('Relative position $\frac{y}{k_R}$','Interpreter','latex','FontSize', 30);
title('Displacement Field','FontSize', 30');
xlim([0 10]);   %set x limits
ylim([-2 0]);   %set y limits
[x,y] = meshgrid(0:0.01:10,0:-0.001:-2); %define the plot domain
u=cos(x).*(exp(0.8475*y)-0.5774*exp(0.3933*y)); % define the x component of the field
v=0.8475*cos(x).*exp(0.8475*y)-1.468*sin(x).*exp(0.3933*y); %define the y component of the field
hFig2=figure(2);
set(hFig2, 'Position', [0 0 1500 750])
contourf(x,y,(u.^2+v.^2).^0.5,100,'LineColor','none') % plot scalar field
c=colorbar; %draw color bar
set(gca,'fontsize',30);
xlabel('Relative position $\frac{x}{k_R}$','Interpreter','latex','FontSize', 30');
ylabel('Relative position $\frac{y}{k_R}$','Interpreter','latex','FontSize', 30);
title('Displacement Module','FontSize', 30');
ylabel(c,'Total displacement $\frac{|\mathbf u|}{k_R}$','Interpreter','latex','FontSize', 30); %color bar label
```

isotropic.m

The solution of band structure for infinite grating is realized with the following matlab script:

```
hFig1=figure(1);    %define new plot window
set(hFig1, 'Position', [0 0 1500 750]); %set plot windows
h=ezplot('cos(x*pi)=cos(y*pi)/0.8')
grid on;
set(h,'LineWidth',2,'linecolor','blue')
set(gca,'fontsize',30); %set plot font size
xlabel('wave solution $\mbox{Re}\left\{\frac{\gamma p}{\
    pi}\right\}$','Interpreter','latex','FontSize', 30');
ylabel('Incident wavenumber $\frac{kp}{\pi}$','
    Interpreter','latex','FontSize', 30);
title('Pass Band','FontSize', 30');
xlim([0 3]);   %set x limits
ylim([0 3]);   %set y limits
hFig2=figure(2);    %define new plot window
set(hFig2, 'Position', [0 0 500 750]); %set plot windows
hold on;
grid on;
h1=ezplot('cos(i*x*pi)=cos(y*pi)/0.8')
set(h1,'LineWidth',2,'linecolor','blue')
h2=ezplot('cos(i*x*pi)=-cos(y*pi)/0.8')
set(h2,'LineWidth',2,'linecolor','blue')
set(gca,'fontsize',30); %set plot font size
xlabel('Attenuation $\mbox{Im}\left\{\frac{\gamma p}{\pi
    }\right\}$','Interpreter','latex','FontSize', 30');
ylabel('');
title('Stop band','FontSize', 30');
xlim([0 1]);   %set x limits
ylim([0 3]);   %set y limits
```

band.m

The plot of refectivity in function of the ratio $\frac{h}{\lambda}$ is done with the following matlab script:

```
x=[0:0.0001:0.05];
 hFig1=figure(1);
     set(hFig1, 'Position', [0 0 800 400]);
set(gca,'fontsize',20);
hold on;
grid on;
plot(x,tanh(100*(0.001+0.5*x)),'linewidth',2,'color','
    Green');
plot(x,tanh(250*(0.001+0.5*x)),'linewidth',2,'color','Red
    ');
plot(x,tanh(500*(0.001+0.5*x)),'linewidth',2,'color','
    Blue');
xlim([-0.01 0.05]);
ylim([0 1.1]);
xlabel('Ratio $\frac{h}{\lambda}$','Interpreter','latex',
    'FontSize', 20');
ylabel('Reflectivity $\tanh(N|r|)$','Interpreter','latex'
    ,'FontSize', 20');
legend('N=100','N=250','N=500','Location','East')
```

thickness.m

The data treatment for time resolved measures is shown in this matlab script:

```
clear %clear the previous data
numfiles = 51; %number of files to read
t_min=975;  %start time measure to plot
t_max=2000; %end time measure to plot
mydata = cell(1, numfiles); %data structure

%import data
for k = 1:numfiles
  myfilename = sprintf('delay_%d.csv', k+1);
  mydata{k} = importdata(myfilename, ',', 2);
end

%data envelope
for i=1:numfiles
 eval(sprintf('s(%d,:)=abs(hilbert(mydata{%d}.data(:,2)))
   ;', i, i));
end

%data conversion in logaritmic scale
for i=1:2000
    for j=1:numfiles
     s(j,i)=10*log10(s(j,i));
    end
end

%data flying mean (smoothing)
for i=1:numfiles
    s(i,:)=smooth(s(i,:),30);
end

%organizing data in matrix
t=zeros(t_max-t_min+1,1);
s2=zeros(numfiles,t_max-t_min+1);
for i=1:t_max-t_min+1
     s2(:,i)=s(:,i+t_min-1);
     t(i,1)=mydata{1}.data(i+t_min-1,1)*10^9;
end
f=zeros(numfiles,1);
for i=1:numfiles
    f(i,1)=345+(i-1)*0.5;
end

%3D plot
hFig1=figure(1);
set(hFig1, 'Position', [0 0 1000 500])
surf(t(:,1),f(:,1),s2,'EdgeColor','none')
hold on;
[~,h] = contourf(t(:,1),f(:,1),s2,100,'LineColor','none')
   ;
xlabh = get(gca,'xLabel');
```

```
49 set(get(gca,'ylabel'),'rotation',45,'FontSize',20);
50 title('Time Resolution of 1 Volt 200ns Pulse Signal');
51 xlabel('Time (ns)');
52 ylabel('Frequency (MHz)');
53 zlabel('Transmitted Signal (dB)');
54
55 hh = get(h,'Children');    %# get handles to patch
       objects
56 for i=1:numel(hh)
57     zdata = ones(size( get(hh(i),'XData') ));
58     set(hh(i), 'ZData',-40*zdata)
59 end
60 view([15 20]);
61 c=colorbar;
62 ylabel(c,'Voltage Loss (dB)');
63
64 %2D plot
65 hFig2=figure(2);
66 set(hFig2, 'Position', [0 0 1000 500])
67 contourf(t(:,1),f(:,1),s2,100,'LineColor','none');
68 xlabel('Time (ns)');
69 ylabel('Frequency (MHz)');
70 title('Time Resolution of 1 Volt 200ns Pulse Signal');
71 c=colorbar;
72 ylabel(c,'Voltage Loss (dB)');
```

impulse.m

BIBLIOGRAPHY

[1] R. P. Feynman, R. B. Leighton, and M. Sands. *The Feynman Lectures on Physics*, volume II. PEARSON Addison-Wesley, 1990.

[2] L. D. Landau and E. M. Lifšic. *Theory of Elasticity*. Pergamon Press, 2 edition, 1970.

[3] L. D. Landau, E. M. Lifšic, and L. P. Pitaevskii. *Electrodynamics of Continuous Media*. Butterworth-Heinemann, 2 edition, 1984.

[4] R. Manenti. Surface Acoustic Wave Resonators for Quantum Information. Master's thesis, 2013.

[5] D. Morgan. *Surface Acoustic Wave Filters*. Academic Press, 2 edition, 2007.

[6] V. Piefort. *Finite Element Modelling of Piezoelectric Active Structures*. PhD thesis, 2001.

[7] M. J. A. Schuetz, E. Kessler, G. Giedke, L. M. K. Vandersypen, M. D. Lukin, and J. I. Cirac. Universal Quantum Transducer based on Surface Acoustic Wave. *Phys. Rev. X*, 5(031031), 2015.

[8] J. Yang. *An Introduction to the Theory of Piezoelectricity*. Springer, 2005.